Journal of Fluids and Structures (2000) **14,** 853–882
doi:10.1006/jfls.2000.0303, available online at http://www.idealibrary.com on IDEAL®

NUMERICAL STUDY OF THE FLOW PAST A CYLINDER EXCITED TRANSVERSELY TO THE INCIDENT STREAM. PART 2: TIMING OF VORTEX SHEDDING, APERIODIC PHENOMENA AND WAKE PARAMETERS

P. ANAGNOSTOPOULOS

Department of Civil Engineering, University of Thessaloniki, Thessaloniki 54006, Greece

(Received 21 September 1998, and in final form 15 March 2000)

In Part 1 of the present study, it was found that the phase angle between the transverse force and the motion of a cylinder subjected to oscillations in the cross-flow direction, is strongly dependent on the parameters of the cylinder excitation. Since the phase angle is associated with the timing of vortex shedding, i.e., the phase of vortex formation with respect to the cylinder motion, the alteration of the phase angle at different conditions of forced excitation suggests a change in timing. For the investigation of timing at different excitation conditions, a detailed numerical visualization in the near-wake was conducted, by superimposing the vorticity contours on the streamlines when the cylinder displacement had reached the uppermost position. Flow visualization during a half-cycle for characteristic cases of the cylinder excitation was also performed, in an attempt to explain the alterations induced in the vortex spacing by the cylinder motion, which were also observed in Part 1. The numerical solution revealed a switch in timing when the excitation frequency is increased over the natural shedding frequency, which is accompanied by an instability in the near-wake which renders the wake aperiodic. Various examples of aperiodic flows are illustrated, and an explanation for the initiation of aperiodicity is provided. Finally, a balance between the circulation shed into the wake per oscillation cycle and that surviving in the vortices is conducted, while the distribution of u'_{rms} along the wake centreline and the base pressure on the cylinder for various excitation conditions are also presented.

1. INTRODUCTION

IT IS WELL-KNOWN THAT vortex shedding behind a cylinder can be dramatically changed when the cylinder oscillates in the cross-flow direction, at or around the natural vortex-shedding frequency. Numerous studies conducted in the last decades have increased substantially our knowledge on the alteration of the wake structure induced by forced excitation at or near synchronization. The experiments by Bishop & Hassan (1964), Koopmann (1967), Griffin (1971), Griffin & Ramberg (1974), Ongoren & Rockwell (1988), Williamson & Roshko (1988), and Gu *et al.* (1994), and the computational studies by Meneghini & Bearman (1995), Copeland & Cheng (1995), Lu & Dalton (1996), Anagnostopoulos (1997a) and Akbari & Price (1997) constitute important advances for the understanding of these complicated flow-body interaction phenomena. In Part 1 of this investigation, Anagnostopoulos (2000) conducted a numerical study of flow past a cylinder forced to oscillate transversely to the incident stream, using the finite element technique, at $\mathrm{Re} = 106$. He considered a great number of cases, in which the cylinder oscillation frequency was varied between 80 and 120% of the natural shedding frequency, and the oscillation amplitude was extended to 50% of a cylinder diameter.

0889–9746/00/080853 + 30 $35.00/0

The aforementioned study revealed the alterations induced on the wake geometry and on the hydrodynamic forces for the different parameters of forced excitation. An interesting result was the change of the characteristics of the flow pattern when the oscillation frequency of the cylinder, f_c, was lower than or equal to the natural shedding frequency, f_s, from the cases where $f_c > f_s$. When $f_c \leq f_s$ the vortex wake within the lock-in region was similar to that observed for flow past a fixed cylinder. When f_c was increased over f_s, the solution revealed that the flow was not fully periodic, but periodicity was established after a number of cycles, except for an oscillation amplitude equal to 50% of a diameter, where cycle-to-cycle periodicity was observed. In all cases when the ratio f_c/f_s, denoted as f_r, was greater than 1, the form of the vorticity contours was different from that occurring for $f_r \leq 1$.

In this second part of the study, a detailed flow visualization of the near-wake was conducted, in order to give insight into the alterations induced on the near-wake geometry and on the timing of vortex shedding for various conditions of forced excitation. The superposition of the vorticity contours on the streamlines was thought to be instructive, at the time instant corresponding to the maximum displacement of the cylinder. For some characteristic cases of amplitude and excitation frequency, the vorticity contours and the streamlines over one-half of a cycle were generated. The numerical flow visualization when f_r exceeds 1 confirmed the switch in timing of vortex shedding observed in experimental studies, accompanied by substantial changes in the flow pattern. Special attention was given to flow cases when f_r was higher than 1, and the oscillation amplitudes were kept low. Initially, a visual study over a sequence of successive cycles from the onset of the cylinder oscillation to the inception of aperiodicity is conducted, in an attempt to investigate the manifestations of aperiodicity. In order to confirm the establishment of periodicity at certain number of cycles as suggested by velocity and force traces in the first part of the study, a detailed flow visualization was conducted over consecutive cycles, when the phase of the cylinder motion was maintained constant. Then, the mechanism which generates aperiodicity in this excitation-frequency regime was elucidated, by examining the flow patterns at various instants over a cycle.

The circulation shed per cycle into the wake is compared with that surviving vortex formation, whereas the distribution of the r.m.s. fluctuation of the streamwise velocity on the wake centreline is also presented. Finally, the base pressure on the cylinder for various conditions of forced excitation has been derived, and is displayed in relevant diagrams.

2. NEAR-WAKE GEOMETRY AND TIMING OF VORTEX SHEDDING

In Part 1 of this study, it became evident that the phase angle between the transverse force and the cylinder motion can be significantly altered, when the cylinder oscillates over a wide range of frequencies and amplitudes. Figure 21 of Part 1 shows an abrupt reduction of the phase angle with increasing oscillation amplitude in the low amplitude regime when f_r equals 0·90 and 0·95, which is not the case for $f_r = 1$. A remarkable result is that the phase angle remains constant for $f_r = 0{\cdot}80$. When f_r exceeds 1, no substantial variations of the phase angle were recorded, which exhibits small fluctuations around 30°, a value lower than all cases in which $f_r \leq 1$. The phase angle between the lift force and the cylinder displacement is associated with the timing of vortex shedding, i.e., the phase of vortex formation with respect to the cylinder motion, and the alteration of the phase angle at different conditions of forced excitation suggests a change in timing.

In addition, the longitudinal spacing of vortices, in the range of frequency ratios $f_r \leq 1$ in which regular vortex shedding is observed, exhibits an interesting behaviour. For $f_r = 0{\cdot}80$ the longitudinal spacing is independent of the oscillation amplitude, similarly to the phase angle. For the other frequency ratios examined ($f_r = 1$, 0·95 and 0·90), the longitudinal

spacing decreases with increasing oscillation amplitude, until the amplitude becomes 40% of a cylinder diameter. If the amplitude is increased still further, the longitudinal spacing remains constant. The decrease of the longitudinal spacing with increasing amplitude is milder for $f_r = 0{\cdot}90$, whereas, as stated earlier, no change of the longitudinal spacing is observed for $f_r = 0{\cdot}80$. The flow visualization in the near-wake presented in what follows will contribute to a better understanding of these phenomena. Since the flow pattern when $f_r \leq 1$ is different from the cases when f_r exceeds 1, these two ranges of excitation frequencies will be examined separately.

2.1. Excitation at Frequency Ratios Lower Than or Equal to 1

The vorticity contours superimposed on the streamlines in the near-wake for constant frequency ratio equal to 1 and oscillation amplitudes ranging between 5 and 30% of a cylinder diameter are presented in Figure 1. Throughout the study, the streamlines have been generated with respect to a fixed frame of reference, at the mean position of the body. In all cases the instant is shown at which the maximum cylinder displacement has been reached, whereas periodicity in the flow has been fully established. The cross-hairs depicted on the cylinder cross-section mark the undeflected position of the cylinder. For all amplitudes, a vortex in the process of being shed is observed at the side at which the cylinder has been displaced. When the oscillation amplitudes is kept low, the recirculating region in the streamline pattern behind the cylinder is larger, and the vortex being shed at the upper part of the cylinder is more developed. In Figure 1(d), which correspond to $A/D = 0{\cdot}30$, no closed streamlines are present, whereas the vortex at the upper part of the cylinder has just started to emerge. The timing of vortex formation at the upper part of the cylinder is not greatly dependent on the oscillation amplitude, which is in accord with the small variation of the phase angle with respect to the oscillation amplitude for the frequency ratio examined. Moreover, the longitudinal distance between the vortex emerging at the upper part of the cylinder and that formed below the cylinder is equal for all amplitudes, which is not the case when the longitudinal spacing has been stabilized farther in the wake, as shown in figure 28 of Part 1 of this study.

The equivorticity lines superimposed on the streamlines for $f_r = 0{\cdot}95$ are displayed in Figure 2. The range of oscillation amplitudes is the same as in Figure 1, and the instant shown is when the cylinder reaches its uppermost position as well. Figure 2 shows that for $A/D = 0{\cdot}05$ the centre of the vortex forming at the upper part of the cylinder lies 2·3 cylinder diameters downstream from the cylinder centre. As A/D is increased to 0·10, the corresponding vortex moves towards the cylinder, whereas, for A/D equal to 0·20 and 0·30, the newly forming vortices above the cylinder come still closer, at approximately the same distance from the cylinder. This situation is in accord with the variation of the phase angle with the amplitude of oscillation, which decreases abruptly as the amplitude increased from 5 to 10% of a diameter, and then it undergoes a less steep decrease. Closed streamlines associated with the newly shedding vortices at the upper part of the cylinder, as in Figure 1, are not detected, but they can be seen behind the lower part of the cylinder, for $A/D \leq 0{\cdot}10$. The longitudinal distance between the vortex being shed above the cylinder and that formed below decreases as the amplitude is increased to 0·20 D, and then remains almost insensitive of the amplitude increases. Figure 3(b) portraying the case $f_r = 0{\cdot}95$ and $A/D = 0{\cdot}40$ helps to support this conclusion.

For the investigation of the effect of the oscillation frequency on the flow pattern, an overview of the vorticity contours superimposed on the streamlines is depicted in Figure 3, for constant amplitude equal to 40% of a cylinder diameter, and frequency ratios in the range between 1 and 0·80. Figure 3 reveals that the vortex formation at the upper part of the

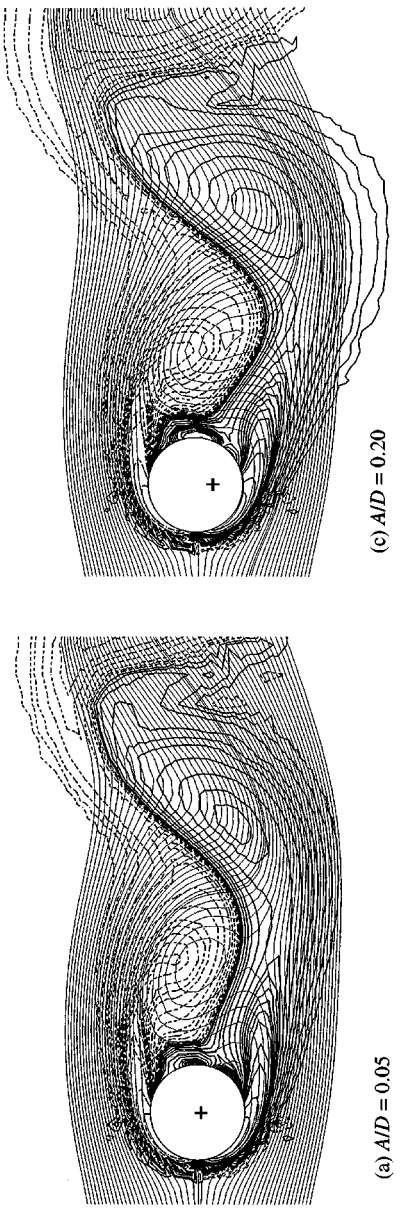

Figure 1. Streamlines and vorticity contours for various oscillation amplitudes, at $f_r = 1$. All frames correspond to maximum displacement of the cylinder, and the cross-hairs mark the undeflected cylinder position.

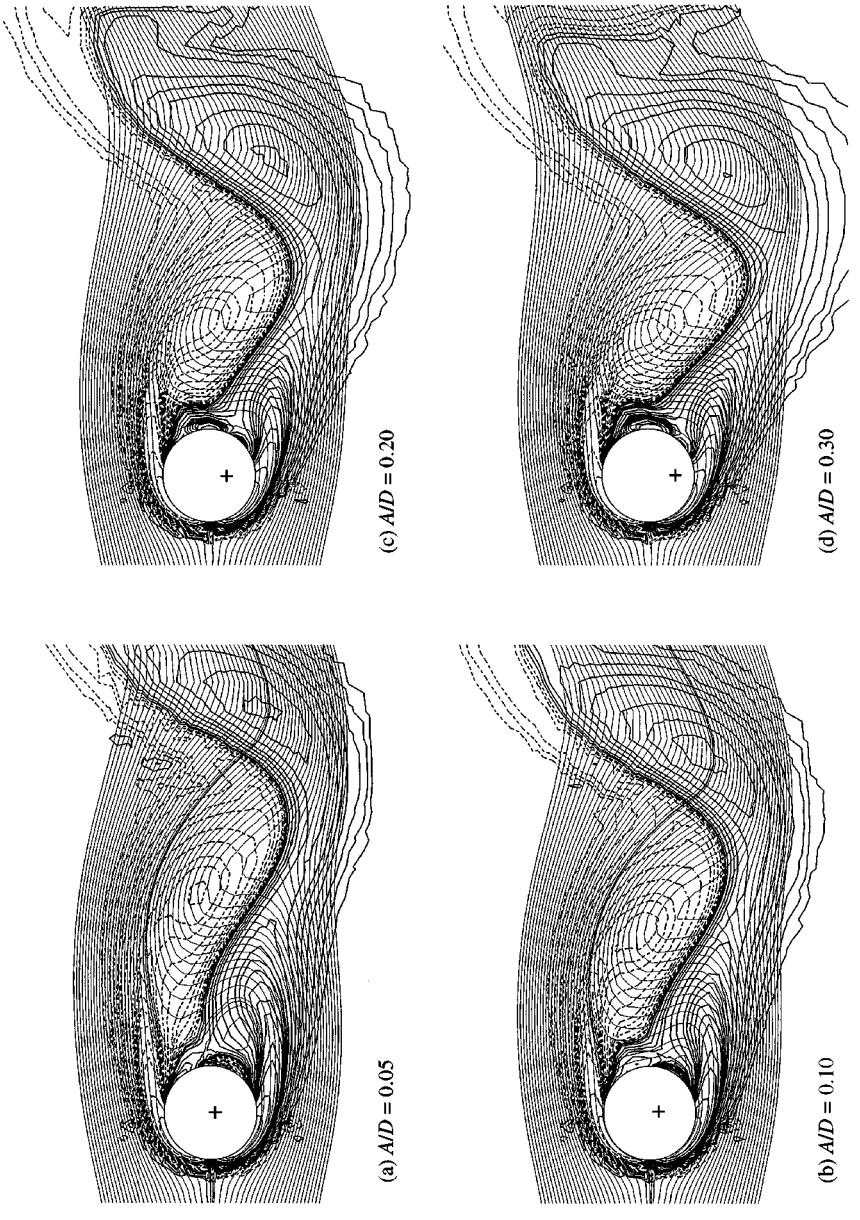

Figure 2. Streamlines and vorticity contours for various oscillation amplitudes, at $f_r = 0{\cdot}95$.

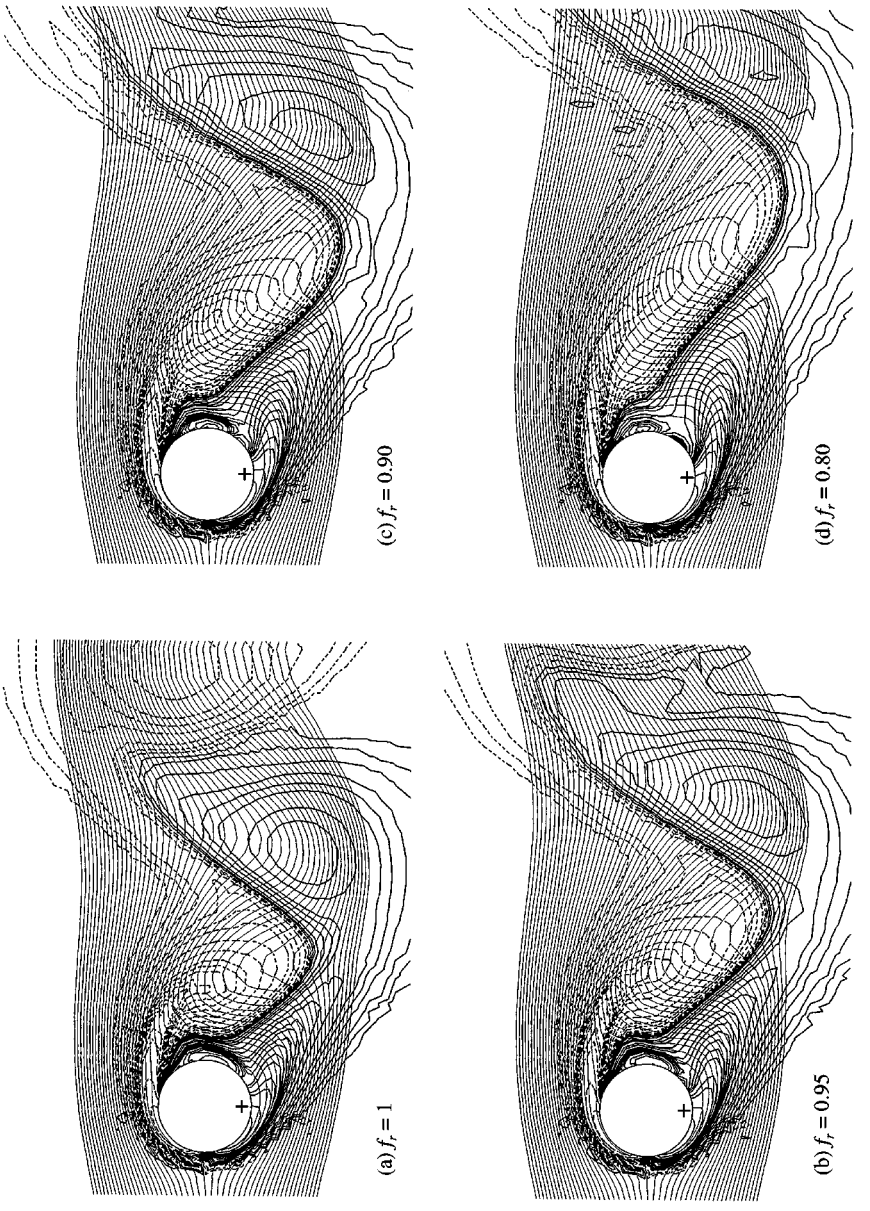

Figure 3. Streamlines and vorticity contours for various oscillation frequencies, at $A/D = 0{\cdot}40$.

cylinder is more advanced as the oscillation frequency decreases. Moreover, an increase in the longitudinal spacing of the vortices in the near-wake is noticeable with decreasing frequency ratio, which displays an almost linear character. These results are in considerable agreement with the experiments by Ongoren & Rockwell (1988) and Gu *et al.* (1994) at higher Reynolds numbers.

For a better interpretation of the flow patterns of Figures 1–3 which correspond to the maximum cylinder displacement, the equivorticity lines and the streamlines over one-half of an oscillation cycles were generated, for some characteristic cases of forced excitation. The equivorticity lines for $f_r = 1$ and $A/D = 0{\cdot}10$ at equal intervals over one half-cycle are depicted in Figure 4, and the corresponding streamlines in Figure 5. Similarly, the equivorticity lines and the streamlines for $f_r = 1$ and $A/D = 0{\cdot}40$ are displayed in Figures 6 and 7, respectively. Comparison of the streamline patterns of Figures 5(a) and 7(a) reveals the existence of an extended recirculating region behind the cylinder formed during the previous half-cycle when $A/D = 0{\cdot}10$, whereas, when A/D equals 0·40, nor recirculating zone is detectable, only an increased streamline spacing in the cross-flow direction can be detected. In spite of this difference, the longitudinal distance between the vortex emerging at the upper part of the cylinder and that formed at the lower part is equal for both amplitudes. This became evident also is Figure 1, in which various oscillation amplitudes are considered, at a constant frequency ratio equal to 1. In the following frames of Figure 5 we can observe the generation of a large streamline bubble behind the cylinder, which is eventually detached as shown in Figure 5(d), and survives until the cylinder reaches its lowermost position. On the other hand, the sequence of frames of Figure 7 shows the formation of a smaller bubble, whose distance from the cylinder in the cross-flow direction increases as the cylinder moves downwards.

As the vortices are displaced downstream in the low-amplitude oscillation, the recirculating region surviving from the previous half-cycle eventually disappears, but as the gap is filled by streamlines, the longitudinal spacing of the vortices increases. This becomes evident from the sequence of streamlines depicted in Figure 5, and from the vorticity contours of the corresponding frames of Figure 4. In Figure 7, which corresponds to $A/D = 0{\cdot}40$, the lack of a recirculating region surviving from the previous half-cycle provides insufficient space for the adjacent vortices to separate from each other as they move downstream, as indicated by the succession of frames in Figure 6. On the other hand, the increased oscillation amplitude in Figures 6 and 7 has as result the increase of the lateral spacing of vortices, compared to that of Figures 4 and 5.

The equivorticity lines and streamlines for $f_r = 0{\cdot}90$ and $A/D = 0{\cdot}10$ are displayed in Figures 8 and 9. Figure 9(a) dictates that when the cylinder reaches its uppermost position, a recirculating bubble has been already developed at the lower part of the cylinder, whereas the vorticity contours of Figure 8(a) portray the formation of a vortex at the upper part of the cylinder, more advanced compared to that of Figure 4(a), when $f_r = 1$. The significant shift of the timing of vortex shedding when f_r is decreased from 1 to 0·90 at $A/D = 0{\cdot}10$, provides an explanation for the increase of the phase angle between the lift force and the cylinder displacement by 80°, as depicted in figure 21 of Part 1 of the study. The following frames of Figure 9 illustrate the increase of the recirculating bubble, which appears more extended compared to the case in which $f_r = 1$. It seems, therefore, that the higher period of the cylinder oscillation with respect to that of natural vortex shedding acts to increase the size of the recirculating zone formed behind the cylinder. This enlarged size of the bubble is the reason for the increased longitudinal spacing of the near-wake vortices compared to the case when $f_r = 1$, since, as obvious from Figures 8 and 9, the spacing between the vortex emerging at the lower side of the cylinder and that formed above the cylinder, is controlled by the extend of the recirculating zone. It should be noted that in the streamline pattern of

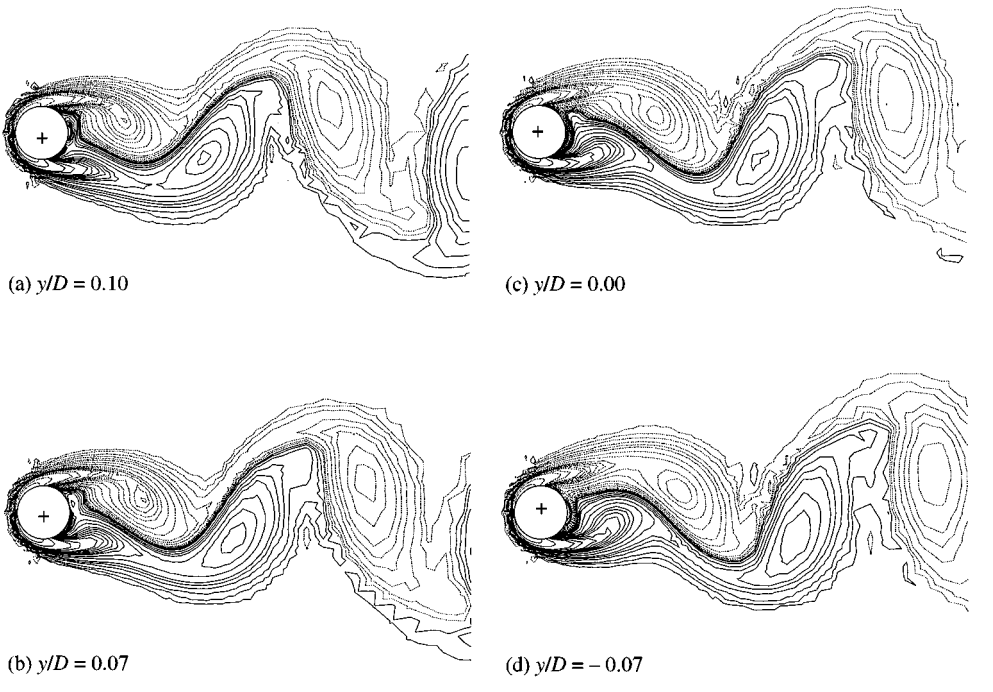

Figure 4. Equivorticity lines over one half of an oscillation cycle; $f_r = 1$ and $A/D = 0{\cdot}10$.

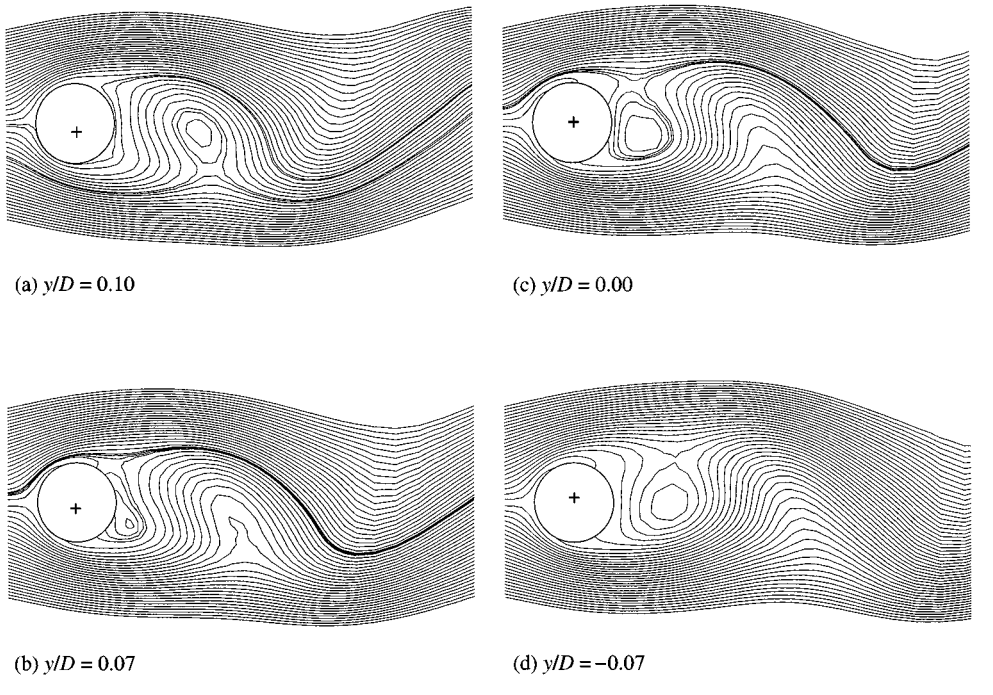

Figure 5. Streamlines over one half of an oscillation cycle; $f_r = 1$ and $A/D = 0{\cdot}10$.

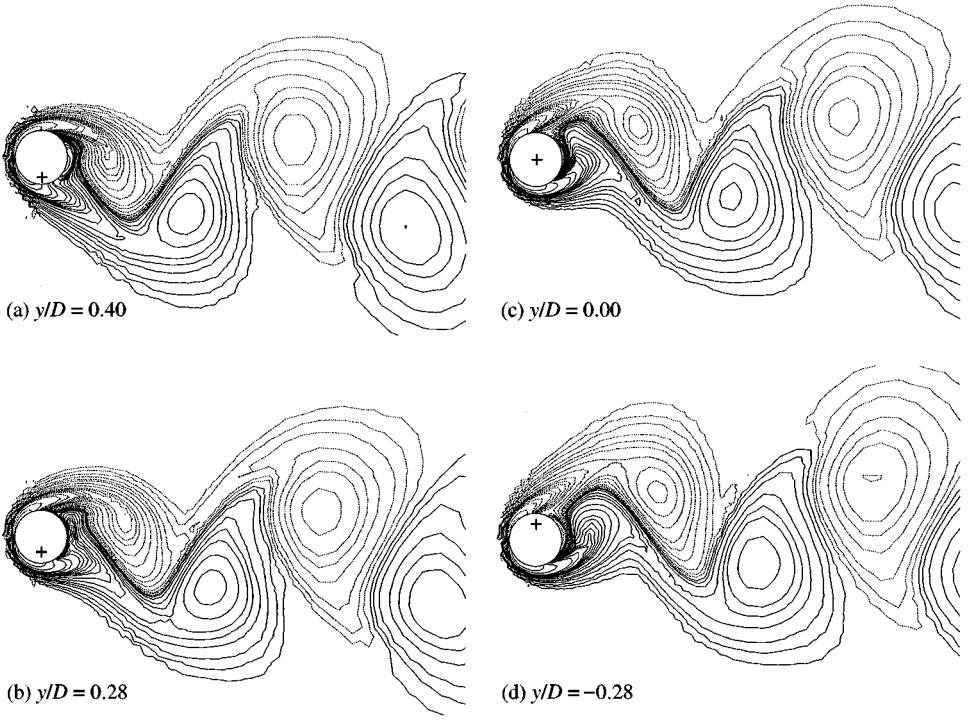

Figure 6. Equivorticity lines over one half of an oscillation cycle; $f_r = 1$ and $A/D = 0{\cdot}40$.

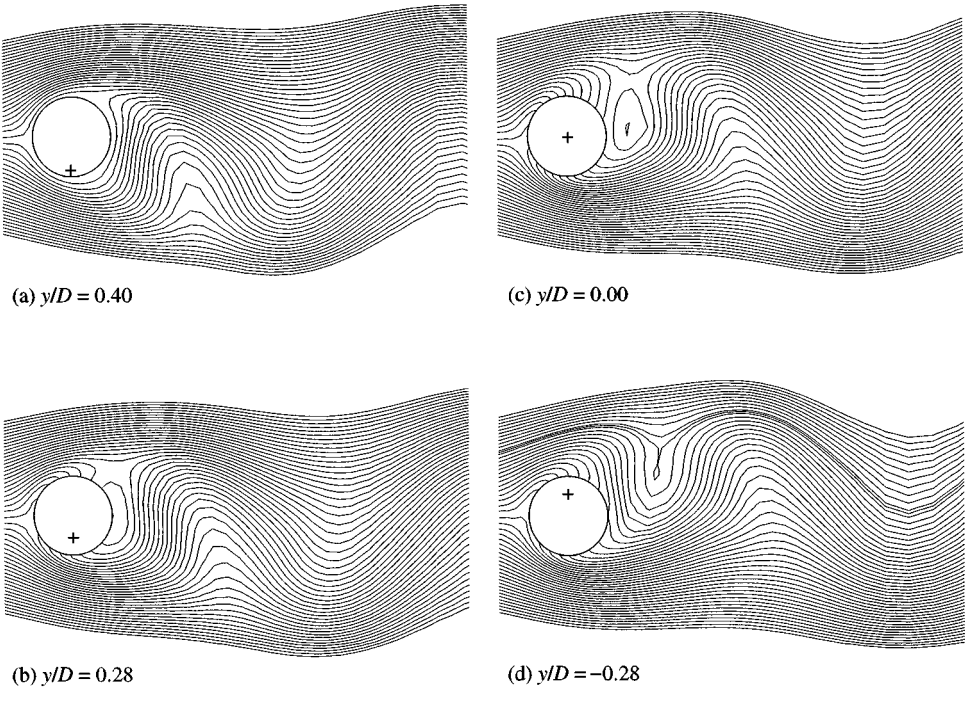

Figure 7. Streamlines over one half of an oscillation cycles; $f_r = 1$ and $A/D = 0{\cdot}40$.

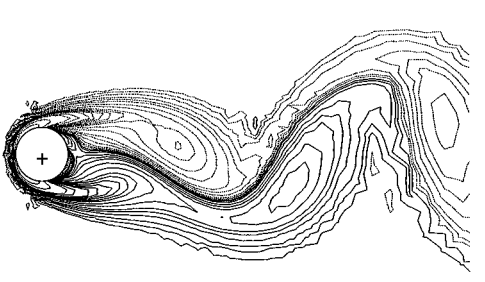

(a) $y/D = 0.10$

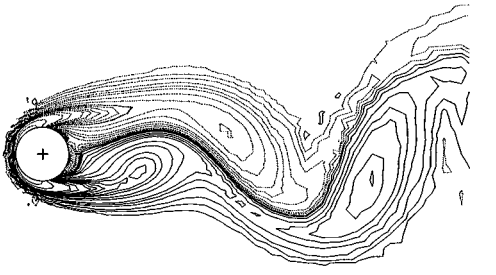

(c) $y/D = 0.00$

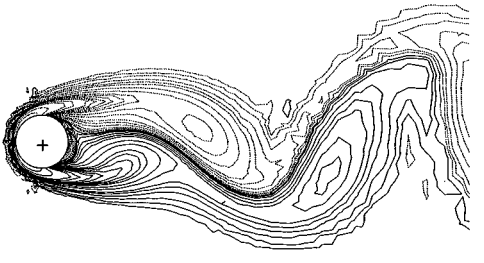

(b) $y/D = 0.07$

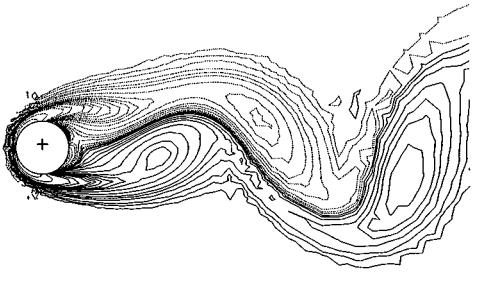

(d) $y/D = -0.07$

Figure 8. Equivorticity lines over one half of an oscillation cycle; $f_r = 0{\cdot}90$ and $A/D = 0{\cdot}10$.

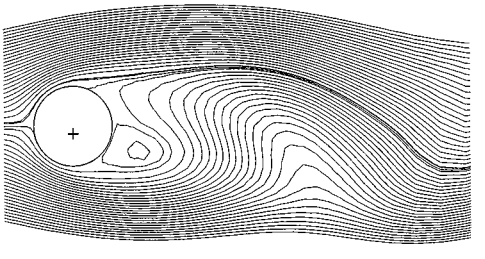

(a) $y/D = 0.10$

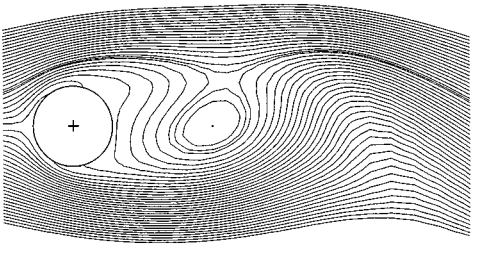

(c) $y/D = 0.00$

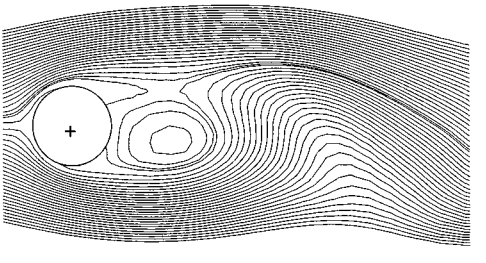

(b) $y/D = 0.07$

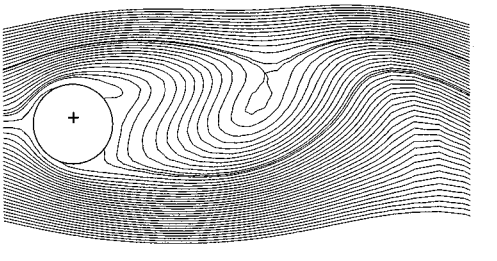

(d) $y/D = -0.07$

Figure 9. Streamlines over one half of an oscillation cycles; $f_r = 0{\cdot}90$ and $A/D = 0{\cdot}10$.

Figure 9(a), contrary to the case of Figure 5(a), no recirculating region detached from the cylinder is detected, but a region of sparsely spaced steamlines is observed, which is dissipated in the following frames.

Similar vorticity contours and streamlines were generated for a wide range of excitation cases, which provide an explanation for the alteration of the longitudinal vortex spacing induced by the various parameters of the cylinder excitation. When the oscillation frequency is decreased at a constant amplitude, an enlarged streamline bubble behind the cylinder is formed during each half-cycle, which induces increased spacing between the newly emerging vortex and that being shed at the opposite side of the cylinder. The spacing between these two vortices remains almost unaltered as the oscillation amplitude is decreased at a constant frequency, but the region of closed streamlines behind the cylinder surviving from the previous half-cycle appears in enlarged form. As the vortices are convected downstream, the augmented recirculating region gradually disappears, causing an increase of the longitudinal spacing of the vortices. It should be noted that, according to figure 28 in Part 1, the longitudinal spacing in the far-wake, remains unaltered as the oscillation amplitude increases from $0{\cdot}40\,D$ to $0{\cdot}50\,D$ for all frequency ratios. Indeed, the near-wake streamlines upon a new vortex formation were equally spaced for both of these amplitudes, producing an increase of the longitudinal spacing with donwstream motion at the same rate. Moreover, the effect of the oscillation amplitude on the extent of the recirculating zone surviving behind the cylinder from the previous half-cycle was less pronounced as the frequency ratio was decreased, until it was almost eliminated for $f_r = 0{\cdot}80$. This is the reason for the milder decrease of the longitudinal spacing with increasing amplitude at $f_r = 0{\cdot}90$, and the constant spacing in the streamwise direction at $f_r = 0{\cdot}80$.

2.2. Excitation at Frequency Ratios Higher Than 1

When the frequency of cylinder oscillation exceeds that of the natural shedding frequency, the situation becomes far more complicated. In Part 1 of the study, it was realized that for $f_r > 1$ the phase angle between the transverse force and the cylinder motion remained almost independent of the excitation parameters. Moreover, the flow was aperiodic at consecutive cycles throughout the oscillation amplitudes considered in the lock-in-region, except for the case $A/D = 0{\cdot}50$. In spite of the periodic character of the wake for $A/D = 0{\cdot}50$, the vorticity contours were markedly different from whose when $f_r \leq 1$. Vortex structure similar to that occurring for $f_r \leq 1$ was observed only for $f_r = 1{\cdot}05$ and $A/D = 0{\cdot}15$, but it was maintained for a limited number of cycles, alternated by a number of consecutive cycles in which an aperiodic wake was observed, until periodicity was reestablished.

The vorticity contours superimposed on the streamlines for f_r equal to 1·05 and 1·20 when $A/D = 0{\cdot}40$ are dispayed in Figure 10. For both frequencies a shedding vortex can be seen from the lower part of the cylinder, although its distance from the cylinder is greater when $f_r = 1{\cdot}05$. A major difference in the streamline patterns of Figure 10 from the corresponding streamlines of Figure 3 when the cylinder oscillated at $f_r \leq 1$ at the same amplitudes, is the existence of two saddle points.[†] Similar phenomena were observed in the numerical study by Lu & Dalton (1996), which also revealed a switch in timing of vortex shedding and two saddle points in the streamlines when f_r was increased to over 1, when the cylinder was forced to oscillate at Reynolds numbers between 185 and 1000. The longitudinal distance between the two saddle points depicted in Figure 10 is greater when $f_r = 1{\cdot}05$, and the orientation of the associated separatrices is different. In Figure 10(a) they

[†] Saddle points are critical points contained in a streamline called "separatrix", as defined by Perry *et al.* (1982).

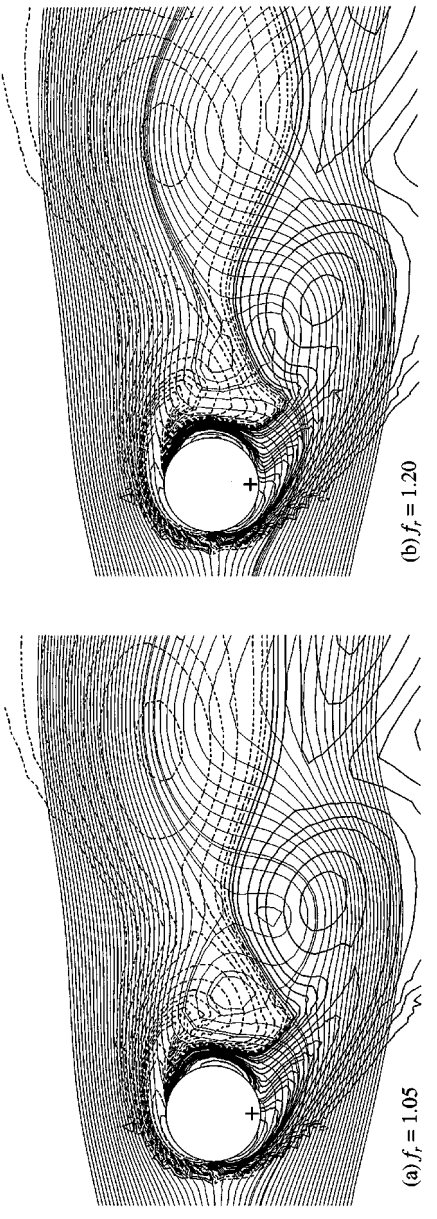

Figure 10. Streamlines and vorticity contours for $f_r = 1{\cdot}05$ and $1{\cdot}20$; $A/D = 0{\cdot}40$.

face downwards and upwards, whereas in Figure 10(b) upstream and downstream. It will be shown later that the streamline configuration in the near-wake is not maintained constant at subsequent cycles, but switches between the cases depicted in Figures 10(a) and 10(b) when the cylinder is excited at constant frequency.

In an attempt to clarify these complicated aperiodic phenomena, the vorticity contours and the streamlines were generated over a large number of oscillation cycles, for various oscillation amplitudes and frequencies exceeding 1. The first case considered was $f_r = 1{\cdot}05$ and $A/D = 0{\cdot}11$, which is the lowest amplitude for which lock-in conditions occur for the frequency ratio under study. Figure 12 of Part 1 revealed a long transient in the hydrodynamic forces at these excitation conditions before quasiperiodicity was established; therefore the examination of the flow pattern within the interval corresponding to the transient was thought to be instructive. The vorticity contours and the streamlines are presented at characteristic periods in Figure 11, at the time instant when the cylinder passes from the undeflected position moving upwards. At the first of the frames shown which corresponds to $t/T_c = 25{\cdot}25$, the vorticity contours depict a fully periodic wake, whereas two saddle points denoted as S_1 and S_2 exist in the streamline pattern. This is the major difference with the streamline pattern of Figure 5(c) for $f_r = 1$ and $A/D = 0{\cdot}10$, where only one saddle points can be seen. It should be reminded than in Figure 5(c) the cylinder passes from the mean position moving downwards, whereas in Figure 11 it is excited upwards. In the following frames of Figure 11, we can observe the increase of the streamline bubble associated with the saddle point S_2 in Figure 11(b), the gradual development of a third saddle point in Figure 11(c), and the significant alteration of the streamline pattern in the near-wake two periods later, in Figure 11(d). These alterations seem to leave the vorticity contours of Figure 11(b) and 11(c) almost unaffected, whereas changes are induced in the vorticity contours of Figure 11(d). After the 37th period the aperiodic regime is initiated. The force traces in figure 12 of Part 1 at similar conditions shown that the lift amplitude and the drag become minimum at $t/T_c = 37$, and afterwards the aperiodic (or quasiperiodic) state is initiated, in agreement with the aperiodic character of the flow pattern.

After the examination of the initiation of aperiodicity, the equivorticity lines for similar excitation parameters over eight consecutive cycles in the aperiodic regime are depicted in Figure 12, and the streamlines in Figure 13. The similarity of Figures 13(a) and 13(h) leads to the conclusion that periodicity is established every eight oscillation cycles. The vorticity contours corresponding to the vortices closer to the cylinder in Figure 12(a) are similar to those of Figure 12(h), in agreement with the eight cycle periodicity of the streamlines depicted in Figure 13. On the other hand, the contours of the vortices near the outflow boundary in Figure 12(a) are similar to the corresponding in Figure 12(g), rather than those in Figure 12(h). It seems, therefore, that a complicated situation occurs, at which low-frequency periodicity in the near-wake is established every eight cycles, whereas in the far-wake every seven cycles. The traces of the hydrodynamic forces depicted in Figure 14 confirm the eight-cycle periodicity detected from the visualization of the flow pattern. As in Part 1, the time base in the force and velocity records is the real time t divided by the cylinder oscillation period, T_c.

The vorticity contours and the streamlines for the case when $f_r = 1{\cdot}05$ and $A/D = 0{\cdot}15$ are depicted in Figures 15 and 16. The flow at these excitation parameters was thought to be of particular interest, since, as stated in Part 1 of the study, periodicity was preserved over a large number of oscillation cycles. A periodic street is observed in the vorticity contours of Figures 15(a) and 15(b) corresponding to the periods between 151 and 157 from the onset of the cylinder oscillation, until a third saddle point develops in the streamline pattern of Figure 16(c). Most of the streamline patterns of Figure 16 in the near-wake are very similar to those obtained experimentally by Gu *et al.* (1994) at Re = 185, although the phase of the

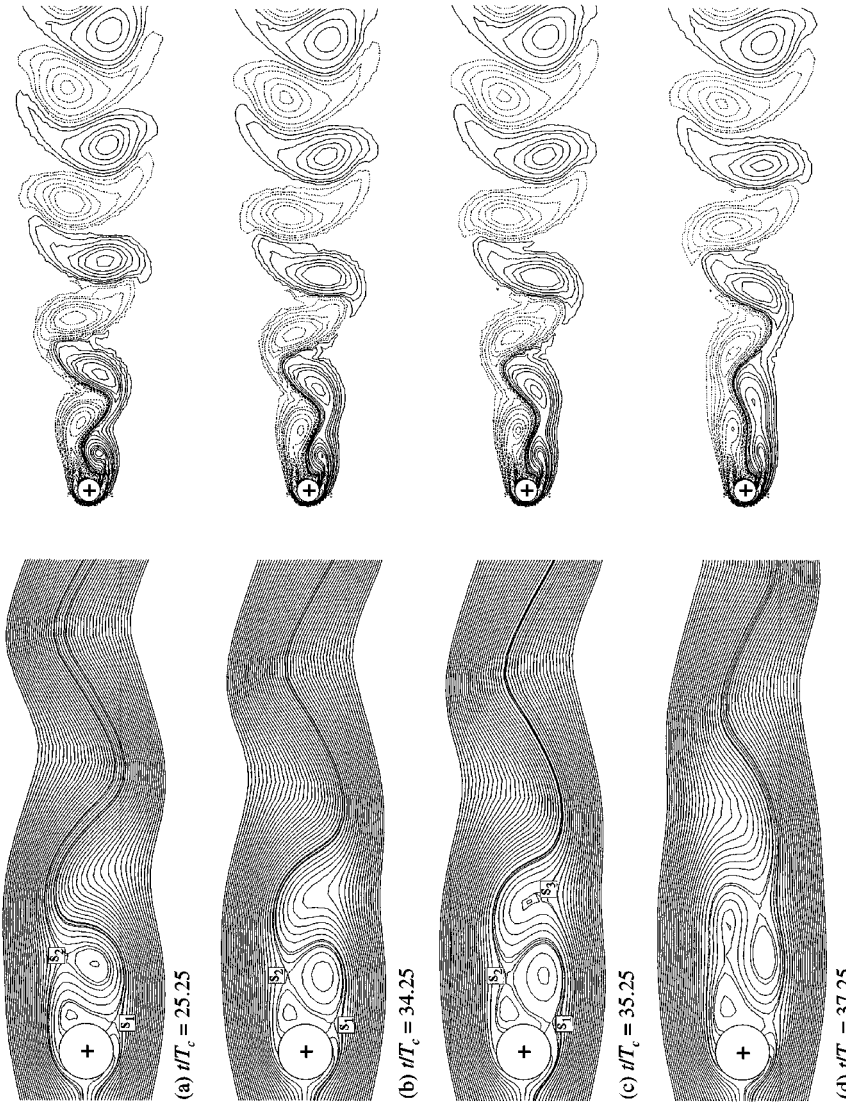

Figure 11. Streamlines (left) and vorticity contours (right) at various cycles for $f_r = 1{\cdot}05$ and $A/D = 0{\cdot}11$; the instant is shown at which the cylinder passes from the undeflected position moving upwards.

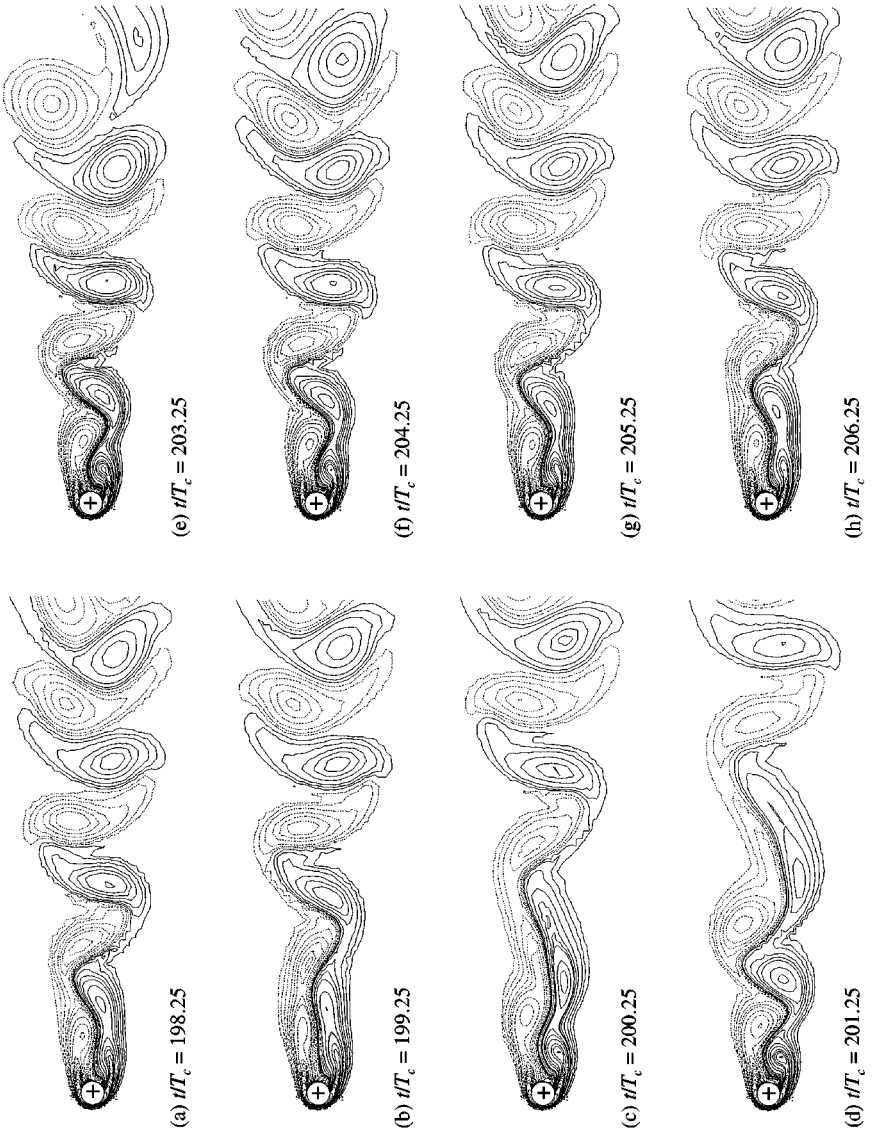

Figure 12. Vorticity contours over eight consecutive cycles for $f_r = 1{\cdot}05$ and $A/D = 0{\cdot}11$.

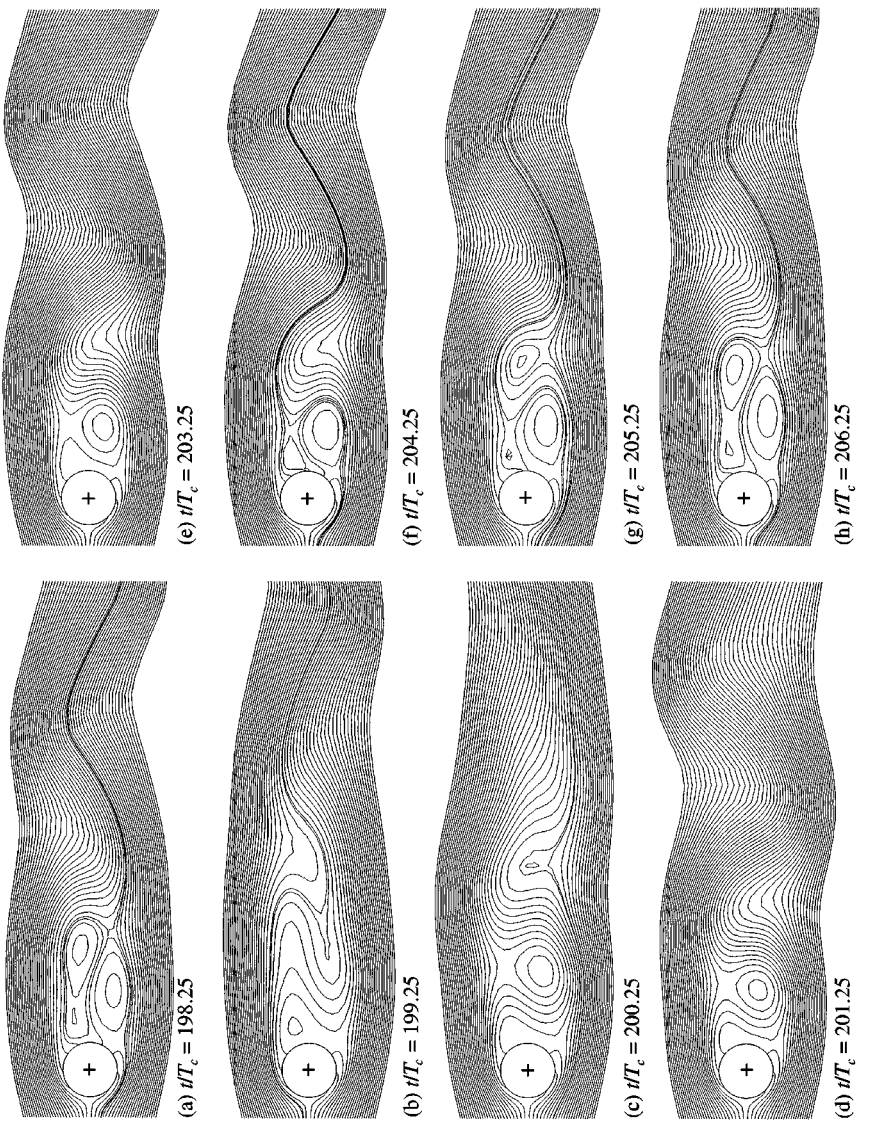

Figure 13. Streamlines over eight consecutive cycles for $f_r = 1{\cdot}05$ and $A/D = 0{\cdot}11$.

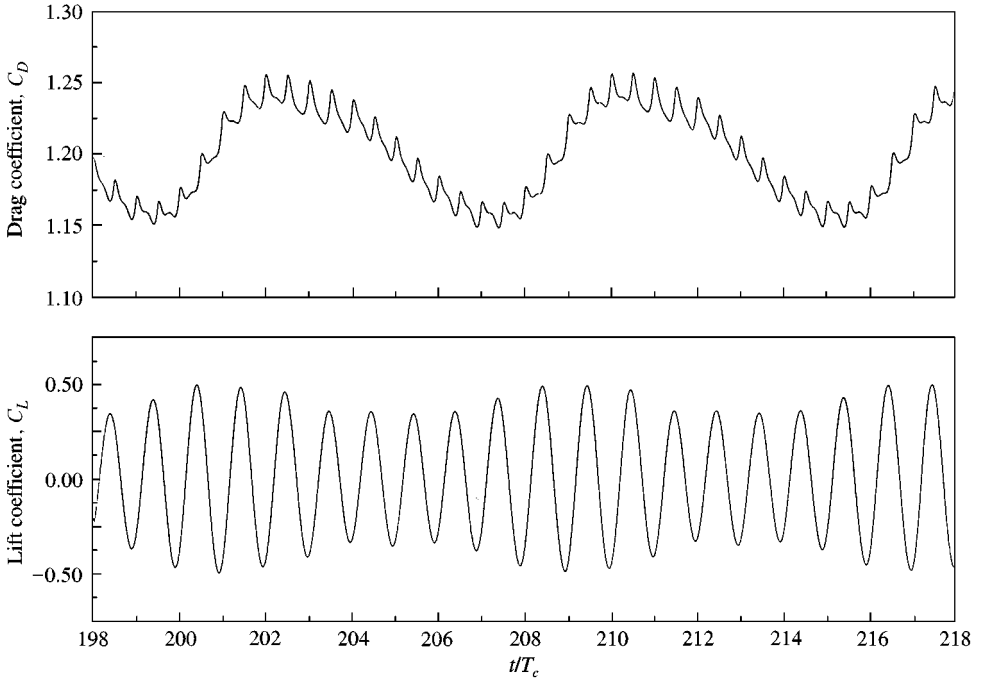

Figure 14. Time history of the hydrodynamic forces for $f_r = 1{\cdot}05$ and $A/D = 0{\cdot}11$.

cylinder motion is not identical in the two studies. As in the case when $A/D = 0{\cdot}11$, the existence of a third saddle point renders the wake aperiodic, as can be seen from the succession of the following frames in Figures 15 and 16. In Figure 16(e) the presence of a fourth saddle point is associated with the vortex pattern of Figure 15(e), in which the vortices are rounder, compared to the vortices of Figure 15(a). In Figure 16(g) only two saddle points are visible, whereas the near-wake streamlines of Figure 16(h) are similar to those in Figure 16(a). After the convection of the vortices existing from previous cycles outside the solution domain, a periodic wake is established again at $t/T_c = 171$. From the force traces of Figure 17 it can be realized that the drag and the lift amplitude become maximum when the corresponding wake pattern is similar to that observed for a fixed cylinder, and the minimum drag corresponds to the pattern, in which the vortices appear in rounded form. Similar fluctuations in the hydrodynamic forces depending on the flow mode have been detected by Copeland & Cheng (1995), who performed computations past a transversely oscillating cylinder at $\mathrm{Re} = 200$.

Honji & Taneda (1968) investigated experimentally the wakes behind a cylinder excited transversely to the incident flow, at Reynolds numbers ranging between 70 and 163. In figure 8 of this study, the far-wake of a cylinder oscillating transversely at $f_r = 1{\cdot}29$ and $A/D = 0{\cdot}20$ is illustrated, for $\mathrm{Re} = 100$. Thus, a numerical simulation at these excitation parameters was conducted, for the sake of complete validation of the present results in the far-wake. Although the solution revealed an aperiodic wake as expected, the physical flow pattern only at one instant is presented, and considerable agreement was observed between a selection of the frames obtained numerically and the experimental flow visualization. Moreover, the numerical study revealed that periodicity was established every three cycles, in agreement with the velocity traces obtained experimentally by Honji & Taneda.

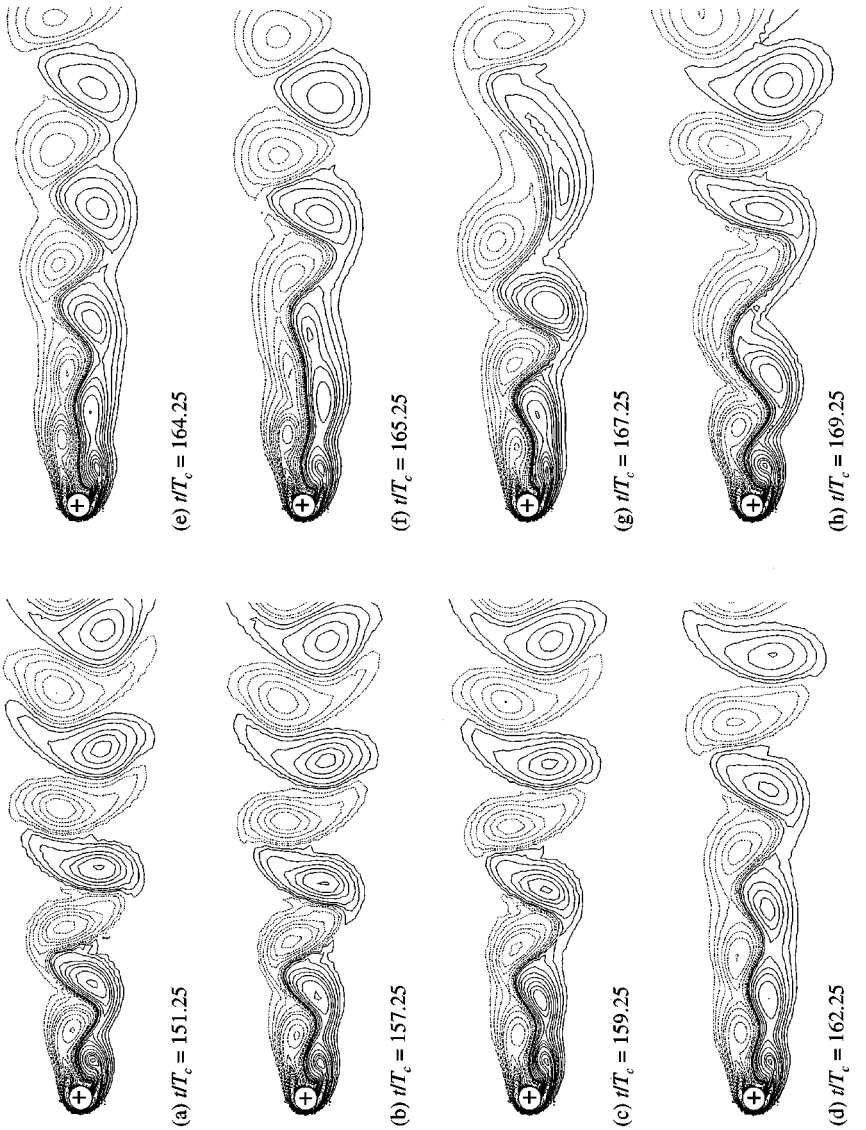

Figure 15. Equivorticity lines at various oscillation cycles for $f_r = 1{\cdot}05$ and $A/D = 0{\cdot}15$

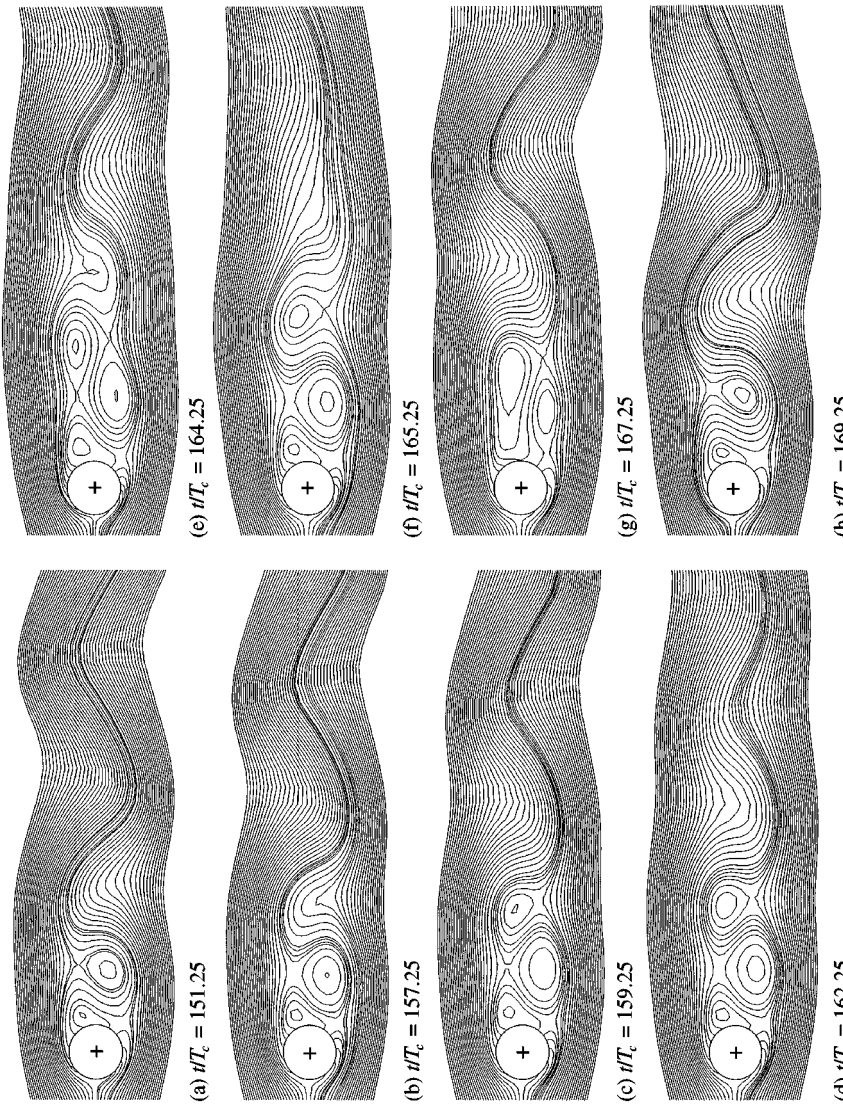

Figure 16. Streamlines at various oscillation cycles for $f_r = 1{\cdot}05$ and $A/D = 0{\cdot}15$.

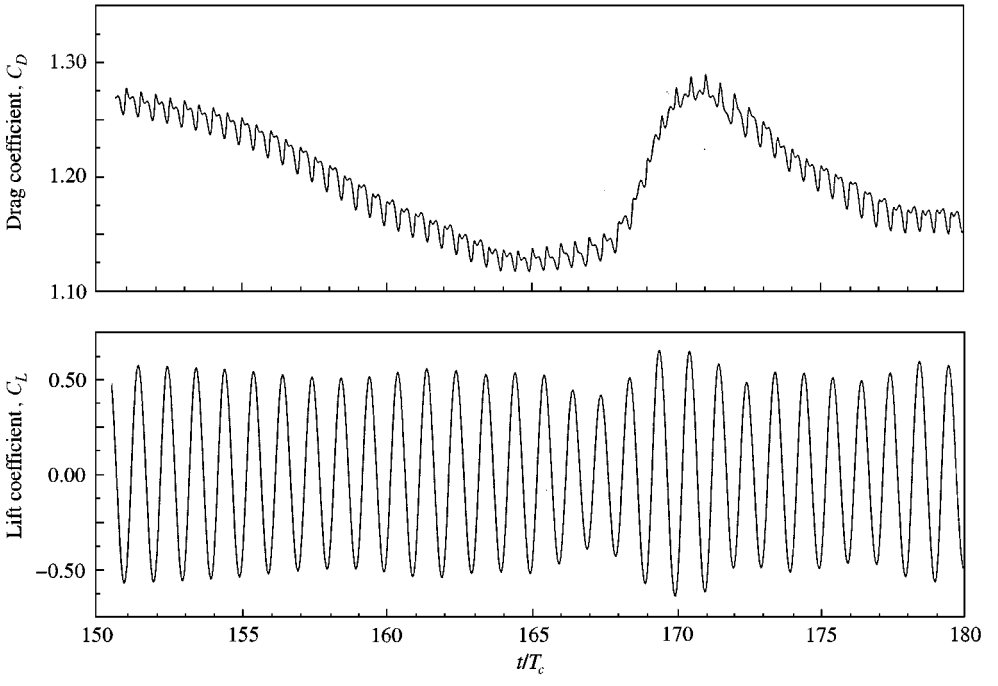

Figure 17. Time history of the hydrodynamic forces for $f_r = 1{\cdot}05$ and $A/D = 0{\cdot}15$.

The previous discussion constitutes a very strong support to the argument proposed in the first part of the study, that the modulation of the force traces when the cylinder oscillation frequency exceeds the natural shedding frequency is a manifestation of an aperiodic wake, rather than unlocked conditions. What requires further investigation is the mechanism that generates the aperiodicity. It became evident earlier that it was initiated when three saddle points were present in the wake. Moreover, it was found that the wake was aperiodic in all cases when f_c exceeded f_s, except for oscillation amplitude equal to 50% of a diameter. In order to investigate possible differences at this amplitude from those at which aperiodicity occurs, the streamlines generated over one cycle for $f_r = 1{\cdot}10$ and $A/D = 0{\cdot}40$ are depicted in Figure 18, and for $f_r = 1{\cdot}10$ and $A/D = 0{\cdot}50$ in Figure 19. Figure 18(a) shows that when the cylinder reaches its maximum displacement, the saddle points S_1 and S_2 coexist in the streamline pattern. As the cylinder passes from the undeflected position moving downwards in Figure 18(b), the saddle points S_2 and S_3 are visible, whereas S_1 has disappeared. The separatrix associated with point S_2 faces downwards, while that associated with point S_3 upwards. As the cylinder reaches its lowermost position in Figure 18(c), a rearrangement of the streamlines in the near-wake has occurred, which altered the orientation of the separatrices. Now the separatrix associated with point S_2 faces downstream, the corresponding associated with point S_3 faces upstream, while fluid originated above the cylinder has occupied the near-wake region, just behind the trailing edge of the cylinder. When the cylinder passes from the undeflected position as it moves upwards in Figure 18(d), a new saddle point denoted as S_4 has been formed; therefore, three saddle points can be noticed. When the cylinder reaches again its uppermost position in Figure 18(f), the streamline pattern is markedly different from that depicted in Figure 18(a) one cycle earlier, which means clearly that periodicity has been disrupted.

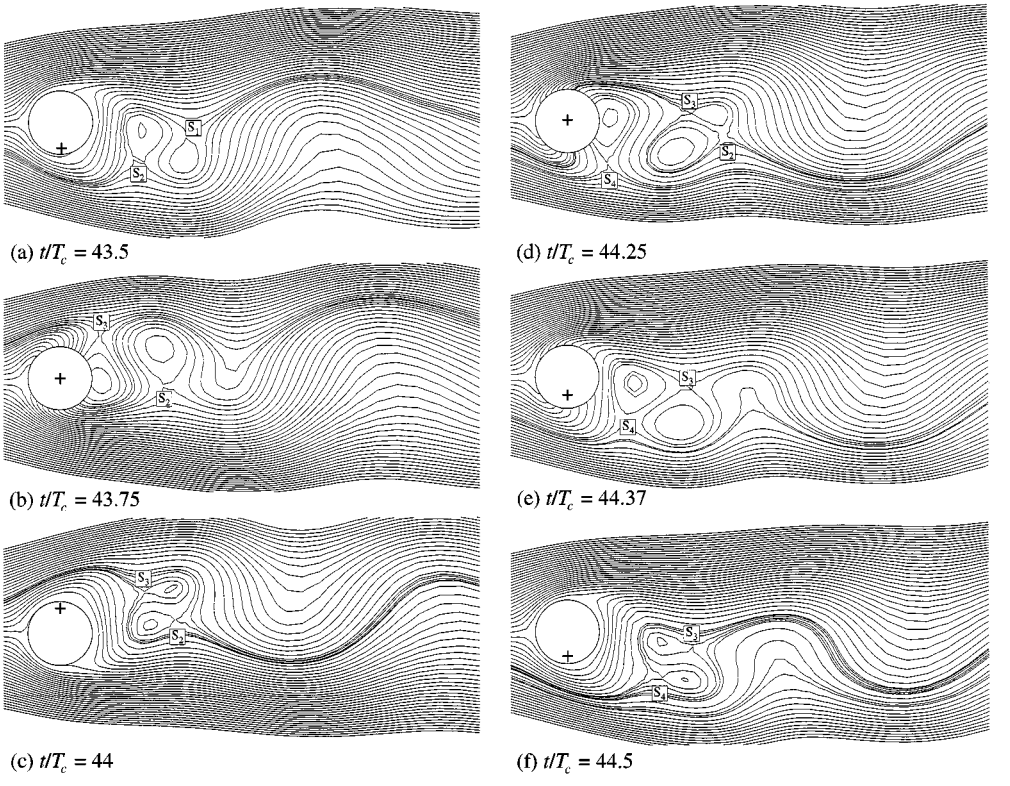

Figure 18. Streamlines over one oscillation cycle; $f_r = 1{\cdot}10$ and $A/D = 0{\cdot}40$.

The sequence of streamlines depicted in Figure 19 over a cycle constitutes a strong evidence that periodicity is preserved. The streamline loop associated with the saddle point S_2 is weaker than its counterpart in Figure 18(b), whereas in Figure 19(c) only one saddle point, denoted as S_3, is detected. Two saddle points are visible in Figure 19(d), which have been reduced to one by the end of the cycle. The flow pattern of Figure 19(c) is a mirror image of that depicted in Figure 19(a) with respect to the wake centreline, whereas the streamlines in Figure 19(f) are similar to those in Figure 19(a), one cycle earlier.

From the comparison of Figures 18 and 19, it seems that the existence of two saddle points when the absolute cylinder displacement becomes maximum, is critical for the generation of aperiodicity. This is equivalent to the development of three saddle points when the cylinder passes from the mean position moving upwards. In such a case an instability is generated, that leads to a streamline pattern which is not the mirror image of that prevailing one half-cycle earlier with respect to the wake centreline. On the other hand, the existence of only one saddle point at the instant when the cylinder displacement has become maximum, acts to preserve the wake periodicity.

The foregoing discussion provides an explanation for the aperiodic character of the flow pattern when f_r exceeds 1. In spite of this aperiodicity at consecutive cycles, a quasiperiodic state is observed, in which periodicity of the flow pattern is established after a number of oscillation cycles, which depends on the excitation parameters. In the sequence of vorticity contours at $f_r = 1{\cdot}05$ and $A/D = 0{\cdot}40$ depicted in figure 26 of Part 1, it was shown that in spite of the cycle-to-cycle aperiodicity, periodicity is established every five cycles, and a merging of adjacent vortices of equal sign occurs.

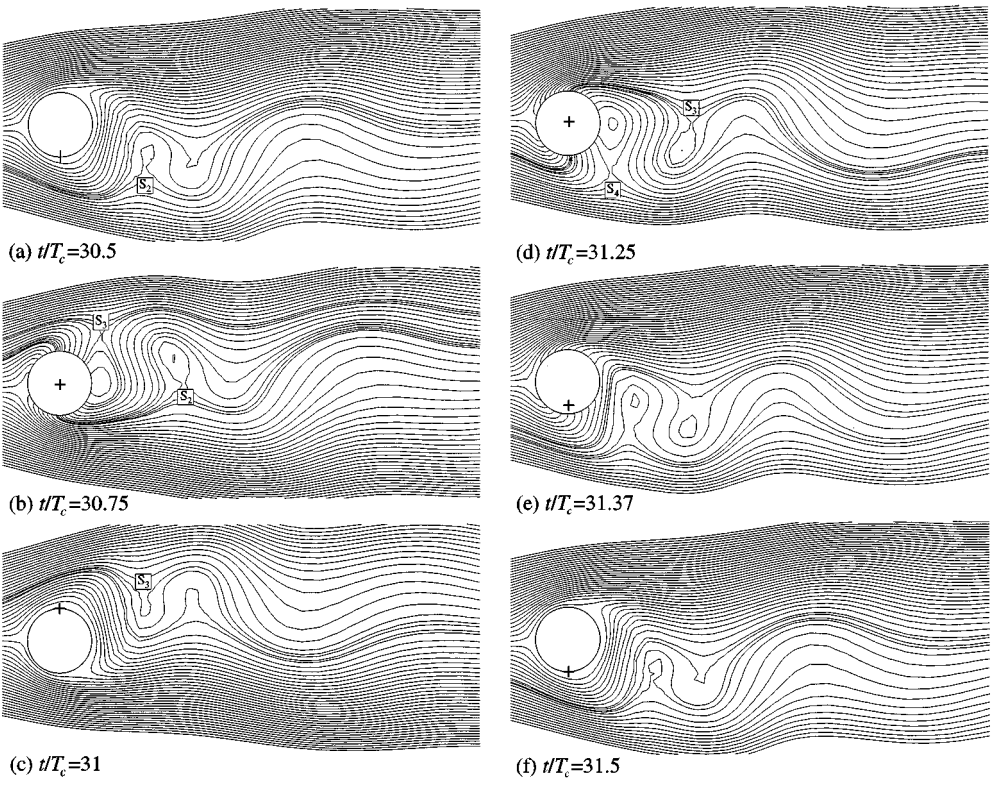

Figure 19. Streamlines over one oscillation cycle; $f_r = 1{\cdot}10$ and $A/D = 0{\cdot}50$.

From the previous reasoning it has become evident that, the frequency ratio at which the switch between the periodic and aperiodic mode occurs, lies between 1 and 1·05 for all oscillation amplitudes considered. A detailed study in this interval has shown that for $A/D = 0{\cdot}20$, the exact frequency ratio at which switch occurs is equal to 1·03. The numerical study by Lu & Dalton (1996) has shown that at Re = 185 the switch frequency ratio is 1·12, in agreement with the experiments by Gu *et al.* (1994), and then decreases to 0·96, when Re becomes equal to 1000. It seems therefore, that the switch frequency ratio is slightly over 1 at Re around 100, becomes maximum at Re around 200 and then decreases continually with increasing Reynolds number.

3. CHARACTERISTIC PARAMETERS IN THE CYLINDER WAKE

3.1. Vortex Strength and Circulation Balance

The determination of vortex strength in the wake of a bluff body has been a very interesting issue. Anagnostopoulos (1997b) determined the vortex strength in the wake of a fixed cylinder from the vorticity distribution obtained numerically. His results were in very good agreement with the experimental measurements by Green & Gerrard (1991) at a similar Reynolds number. He also calculated the circulation shed into the wake during one period and determined the amount of circulation surviving in the vortices

The same technique was used for the determination of the circulation shed per oscillation cycle into the wake when the cylinder oscillates transversely to the incident stream. At each

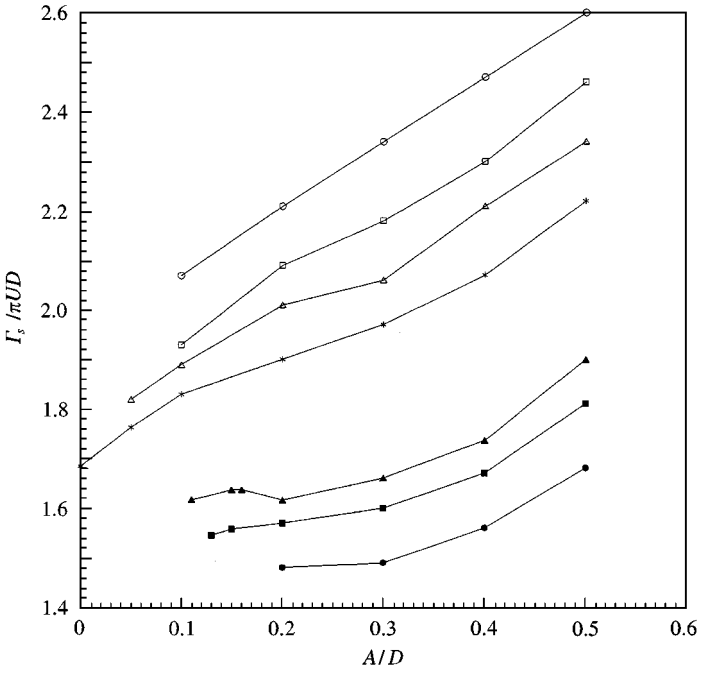

Figure 20. Circulation shed into the wake during one oscillation period for various oscillation amplitudes and frequencies: –○–, $f_c/f_s = 0{\cdot}80$; –□–, $f_c/f_s = 0{\cdot}90$; –△–, $f_c/f_s = 0{\cdot}95$; –∗–, $f_c/f_s = 1{\cdot}00$; –▲–, $f_c/f_s = 1{\cdot}05$; –■–, $f_c/f_s = 1{\cdot}10$; –●–, $f_c/f_s = 1{\cdot}20$.

time level, a line segment perpendicular to the free stream was considered, extending from the separation point A to the outer boundary B. The amount of circulation, Γ_s, passing through the segment AB over a shedding period T_v, was evaluated in terms of the vorticity ζ, from

$$\Gamma_s = \int_0^{T_v} \int_A^B u\zeta \, \mathrm{d}y \, \mathrm{d}t. \tag{1}$$

The only difference from the fixed cylinder case is that, while for a stationary cylinder the fluctuation of the separation angles in a cycle is just 2–3°, when the cylinder oscillates, the fluctuation of the separation angles increases with the oscillation amplitude, and can reach values as high as 50° when the amplitude becomes 50% of a diameter. The circulation shed per cycle normalized by πUD for all cases considered in the lock-in region is depicted in Figure 20. It is clearly seen that for constant oscillation frequency the circulation flux increases with the amplitude, while, when the amplitude remains constant, it increases with decreasing oscillation frequency. This is to be expected, recalling equation (1), since in such a case the shedding period which is equal to the cylinder oscillation period becomes greater, promoting the circulation influx.

The strength of the vortices as function of their downstream distance was calculated at $f_r = 1$ for various oscillation amplitudes. The circulation of each vortex was evaluated from the equivorticity lines, like those depicted in figure 22 of Part 1, using Stokes' theorem between the vorticity and circulation. Since the vortex regions are growing by diffusion as they move downstream, the whole area of each vortex, determined from the outermost contour corresponding to a very low absolute vorticity value, was considered for the derivation of circulation. As in the fixed cylinder case, some uncertainty exists in the

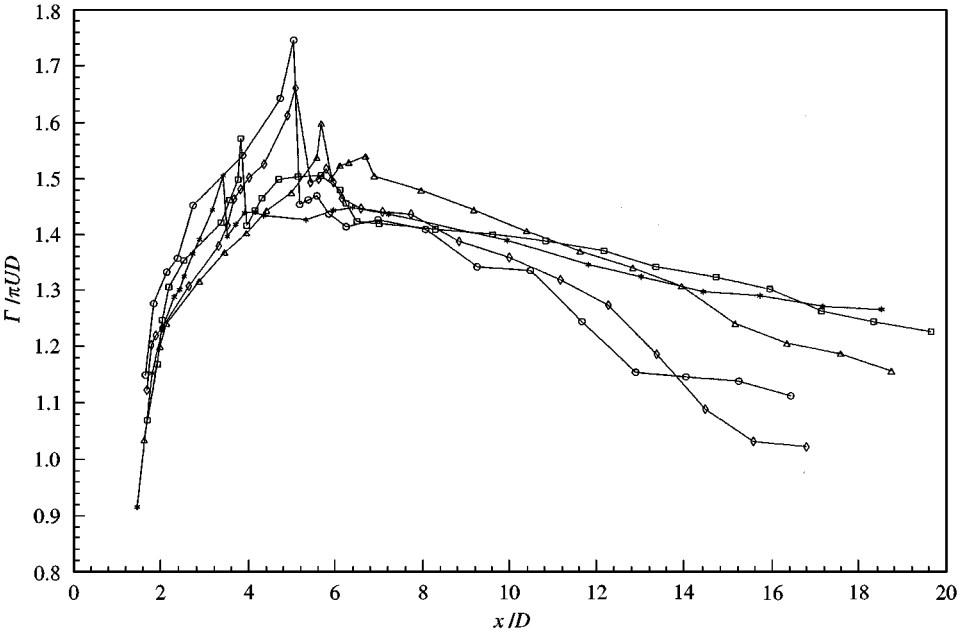

Figure 21. Vortex strength as function of downstream distance from the cylinder, when the cylinder oscillates at $f_r = 1$: –∗–, $A/D = 0{\cdot}10$; –□–, $A/D = 0{\cdot}20$; –△–, $A/D = 0{\cdot}30$; –◇–, $A/D = 0{\cdot}40$; –○–, $A/D = 0{\cdot}50$.

determination of the boundary of the shedding vortex closest to the cylinder, which is not thought to be critical. The values of the vortex strength, normalized by πUD, as a function of the downsteam distance are displayed in Figure 21. The vortex strength increases gradually after formation, acquires its maximum value which increases with increasing oscillation amplitude, and then decreases until the vortex reaches the downstream boundary. Close to the downstream boundary the vortex strength decreases as the amplitude increases to $0{\cdot}30D$, in accord to the vorticity contours depicted in figure 22 of Part 1. When this amplitude is exceeded, the coalescing of vortices close to the downstream boundary leads to increased values of vortex strength when $A/D = 0{\cdot}50$, compared to the case in which $A/D = 0{\cdot}40$.

The rate of circulation contained in the vortices can be expressed as

$$\Gamma f_v = \Lambda U^2, \tag{2}$$

where Γ is the vortex strength, f_v the shedding frequency and Λ a dimensionless parameter. When the oscillations are locked as in the cases considered herewith, f_v coincides with the cylinder oscillation frequency, f_c. From Figures 20 and 21 the circulation balance in the wake for $f_r = 1$ can be summarized in Table 1.

Table 1 indicates that, when the cylinder oscillates, the maximum circulation surviving vortex formation is approximately 80% of that shed into the wake. The value of the dimensionless coefficient Λ increases with increasing oscillation amplitude, when the frequency of oscillation remains constant. The increase of Λ follows the same trend with the results by Griffin & Ramberg (1974) at Re = 144, although the values of Λ in the present study are higher. This is to be expected, since in the present study the maximum circulation was used for the evaluation of Λ, whereas in the study by Griffin & Ramberg the circulation was determined from velocity measurements at the end of the stable region, where the circulation is somewhat lower than maximum.

TABLE 1

Circulation balance in the wake

A/D	Circulation shed per cycle (1)	Maximum strength of vortices (2)	Rate of circulation surviving (2)/(1)	Coefficient Λ in equation (2)
0	1·69	1·23	0·73	0·64
0·1	1·83	1·51	0·83	0·79
0·2	1·90	1·57	0·83	0·82
0·3	1·97	1·60	0·81	0·83
0·4	2·07	1·66	0·80	0·86
0·5	2·22	1·75	0·79	0·91

3.2. DISTRIBUTION OF u'_{rms} ON THE WAKE CENTRE-LINE — LOCATIONS OF MAXIMUM Γ AND u'_{rms}

The distribution of the r.m.s. fluctuation of the streamwise velocity, denoted as u'_{rms}, on the wake centreline, is depicted for various oscillation amplitudes at $f_r = 1$ in Figure 22. The location on the wake centreline where u'_{rms} becomes maximum is one of the criteria for the determination of the vortex formation length. The computational study of Anagnostopoulos (1997b) has shown that, for the flow past a fixed cylinder, the location of maximum u'_{rms} on the wake axis coincides with the downstream distance from the cylinder where the vortex strength becomes maximum. Figure 22 shows that the point where u'_{rms} becomes maximum moves towards the cylinder as the oscillation amplitude increases. On the other hand, Figure 21 dictates that the distance of maximum vortex strength moves downstream as the oscillation amplitude increases, until A/D becomes equal to 0·30. Then it performs a small motion towards the cylinder until the amplitude reaches 50% of a diameter. The location of maximum vortex strength and maximum u'_{rms} on the wake centreline for all amplitudes examined is illustrated in Figure 23. The points of maximum u'_{rms} are very close to the values derived experimentally by Griffin (1971) at $\mathrm{Re} = 120$.

Figure 23 reveals the existence of a jump of the location of maximum vortex strength, as the oscillation amplitude increases from $0{\cdot}20\,D$ to $0{\cdot}30\,D$. An explanation can be give with reference to Figure 1. For $A/D \leq 0{\cdot}20$ a saddle point can be detected in the streamlines, which is not the case for higher oscillation amplitudes. This saddle point is associated with a "neck" in the contours of positive vorticity at the lower part of the cylinder which bound the growing vortex, similarly to the case when the cylinder remains fixed (Anagnostopoulos 1997b). For a better understanding of how the existence of this "neck" affects the location of maximum vortex strength, we consider Figures 4–7. Figure 4(a), when the cylinder oscillates at $A/D = 0{\cdot}10$, corresponds to the instant, at which the strength of the vortex forming below the cylinder has become maximum. After that, a "necking" in the vorticity contours develops, in accord with the gap in the streamlines of Figure 5(b), which causes cut-off of vorticity supply to the vortex. Thus, the strength of the vortex under consideration is reduced as it moves further downstream, due to mutual cancellation of vorticity. On the other hand, when the cylinder oscillates at $A/D = 0{\cdot}40$, it is evident from the streamlines depicted in Figure 7, that a gap similar to that of Figure 5(b) does not exist. The vorticity contours of Figure 6 suggest that, due to the absence of this gap, a continuous supply of positive vorticity occurs to the vortex forming below the cylinder, as the cylinder moves downwards. Switching to the counterpart of this vortex when the cylinder displacement becomes positive, which corresponds to the vortex already formed at the upper part of the cylinder in Figure 6(a), we observe that its strength is maximized, when the shedding of

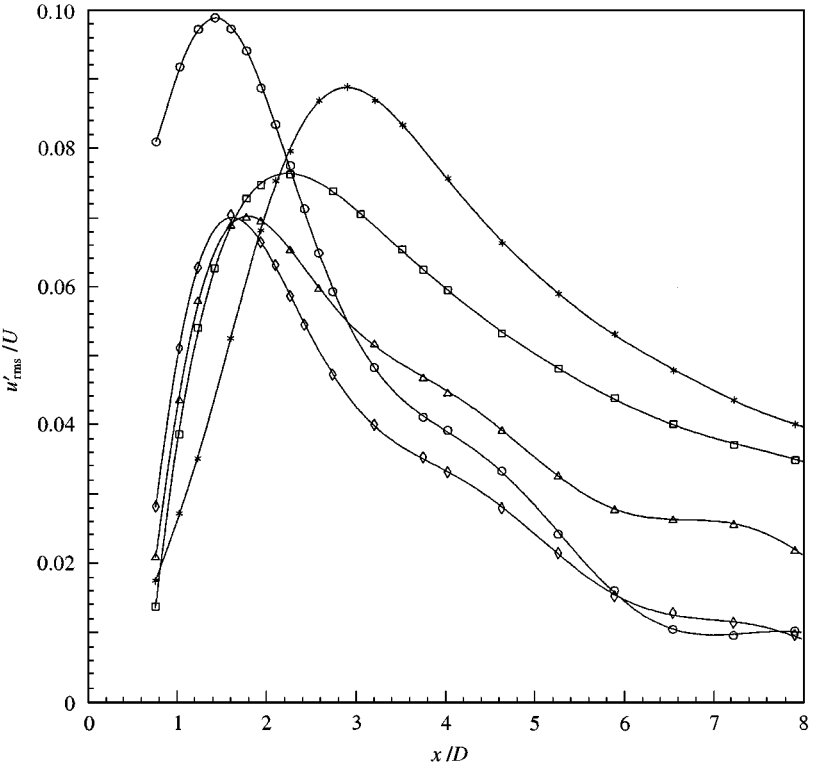

Figure 22. Distribution of the u'_{rms} on the wake centreline, when the cylinder oscillates at $f_r = 1$: –∗–, $A/D = 0{\cdot}10$; –□–, $A/D = 0{\cdot}20$; –△–, $A/D = 0{\cdot}30$; –◇–, $A/D = 0{\cdot}40$; –○–, $A/D = 0{\cdot}50$.

the new vortex from the same part of the cylinder begins. This corresponds to an instant intermeditate of those depicted in Figures 6(a) and 6(b). Then, the feeding of the vortex with circulation from the cylinder is terminated as concluded from the breaking of the outermost vorticity contours, and its strength is reduced as it moves downstream due to mutual cancellation of vorticity.

An explanation of the fluctuation of the position of maximum u'_{rms} on the wake axis can be given with reference to the streamline patterns of Figures 5 and 7, for $f_r = 1$ and A/D equal to 0·10 and 0·40, respectively. In Figure 5(a) an extended region of closed streamlines exists behind the cylinder from the previous half-cycle, whose size reduces gradually in the following instants, until it is eliminated in Figure 5(d). The location where this happens corresponds to the point of maximum u'_{rms}, since the smaller transverse spacing of streamlines, implies higher velocities and higher velocity fluctuations over a cycle. On the other hand, Figure 7(a) shows no recirculating region existing in the near-wake from the previous half-cycle, whereas a streamline bubble starts to develop in Figure 7(b), which is almost dissipated by the end of the half-cycle, as shown in Figure 7(d). The lack of recirculating velocities in Figure 7(a) produces a peak of the u'_{rms} close to the cylinder, at a location which corresponds approximately to the streamwise distance of the centre of the newly emerging vortex at the upper part of the cylinder, as shown in Figure 6(b).

Flow visualization at other oscillation amplitudes for $f_r = 1$ confirmed the dependence of the point of maximum u'_{rms} on the wake axis on the extent of the separated region behind the cylinder. It seems therefore, that although at low amplitudes the location of maximum u'_{rms} on the wake axis gives a measure of the extent of the formation region as in the case when

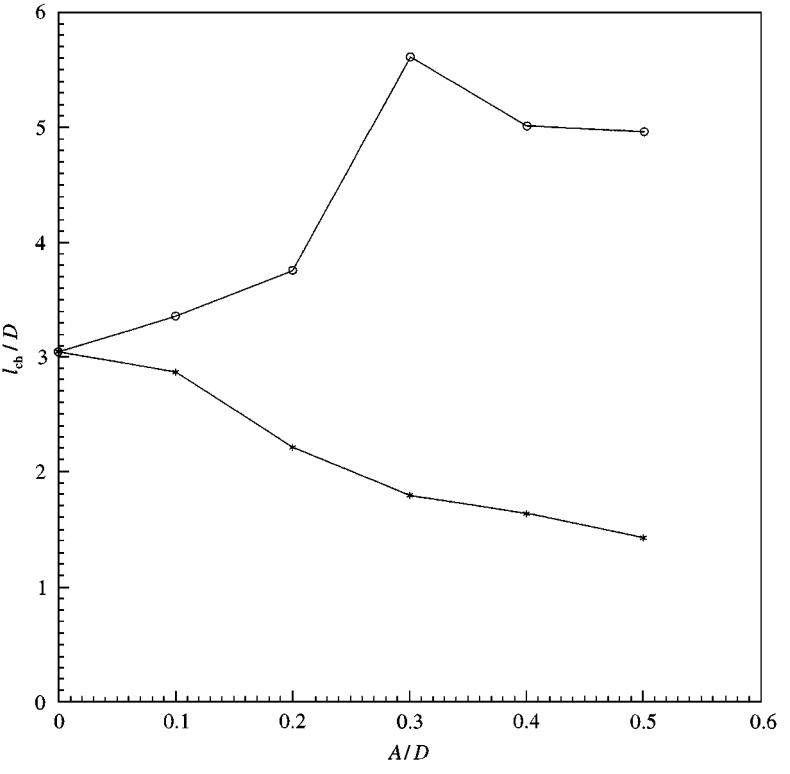

Figure 23. Location of maximum vortex strength and maximum u'_{rms} on the wake centreline, when the cylinder oscillates at $f_r = 1$: −○−, Maximum vortex strength; −∗−, maximum u'_{rms}.

the cylinder is held fixed, at high amplitudes it provides an estimate of the first appearance of the vortices.

From the previous discussion it has become evident that the position of maximum u'_{rms} on the wake centreline does not coincide with the location of maximum vortex strength when the cylinder oscillates, therefore the definition of the vortex formation length based on these quantities is rather trivial.

3.3. Base Pressure on the Cylinder

The base pressure for A/D equal to 0·20 and 0·40 normalized by the base pressure for a fixed cylinder, C_{pbo}, is depicted in Figure 24. The computed value of C_{pbo} is equal to $-0{\cdot}77$. For a constant amplitude, the absolute base pressure increases as the oscillation frequency is increased to a value equal to the natural shedding frequency. Then it experiences an abrupt decrease, and rises again as the oscillation frequency is increased still further. For the same oscillation frequency, the absolute base pressure is greater when the cylinder is oscillating at a higher amplitude. The experimental values by Stansby (1976) at $\mathrm{Re} = 8600$ follow a similar trend, although the absolute base pressure values are higher than in the present study. The effect of the oscillation amplitude on the base pressure when the frequency is maintained constant is portrayed in Figure 25. In all cases the increase of the oscillation amplitude acts to increase the absolute value of base pressure. This is in agreement with the mean drag values presented by Anagnostopoulos (1999) in figure 19 of Part 1 of the study.

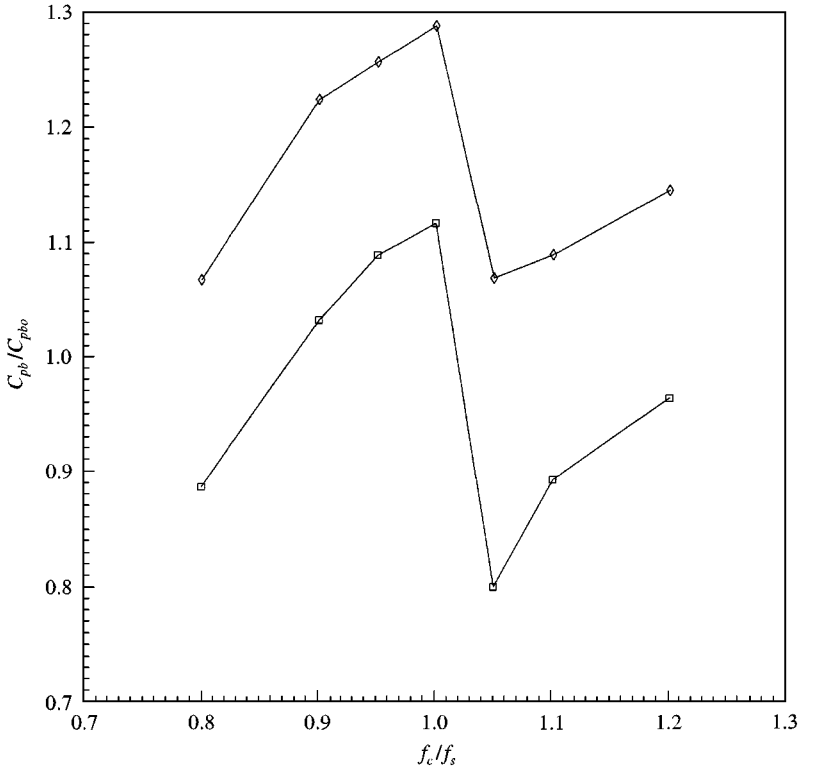

Figure 24. Base pressure as function of the cylinder oscillation frequency. The corresponding base pressure for fixed cylinder, C_{pbo}, is equal to $-0{\cdot}77$: –□–, $A/D = 0{\cdot}20$; –◇–, $A/D = 0{\cdot}40$.

4. CONCLUSIONS

In this second part of the study, a detailed flow visualization of the near-wake was conducted, in an attempt to interpret the fluctuations of the phase angle between the transverse force and the cylinder motion, and the alterations induced in the wake geometry for various conditions of forced excitation. The flow visualization revealed that, when the cylinder oscillates at a constant frequency ratio lower than or equal to 1, the formation of the newly shedding vortex when the cylinder displacement becomes maximum is more advanced as the oscillation amplitude is decreased, the difference in timing being more pronounced at frequency ratios lower than 1. On the other hand, when the oscillation amplitude is maintained constant, the decrease of the oscillation frequency advances the formation of the new vortex at maximum cylinder displacement.

The flow visualization over one half-cycle demonstrated the role of the streamline bubble formed behind the cylinder during this interval, which increases in size and is detached earlier from the cylinder as the oscillation frequency is reduced. The size of this bubble seems to control the longitudinal spacing of vortices in the immediate vicinity of the cylinder. On the other hand, the extent of the recirculating region behind the cylinder surviving from the previous half-cycle, varies inversely with the oscillation amplitude at constant frequency. The augmented recirculating region prevailing at low amplitudes, acts to increase the longitudinal vortex spacing farther in the wake.

When the oscillation frequency exceeds the natural shedding frequency, the flow pattern is drastically altered. A switch in timing of vortex shedding occurs, whereas the flow is

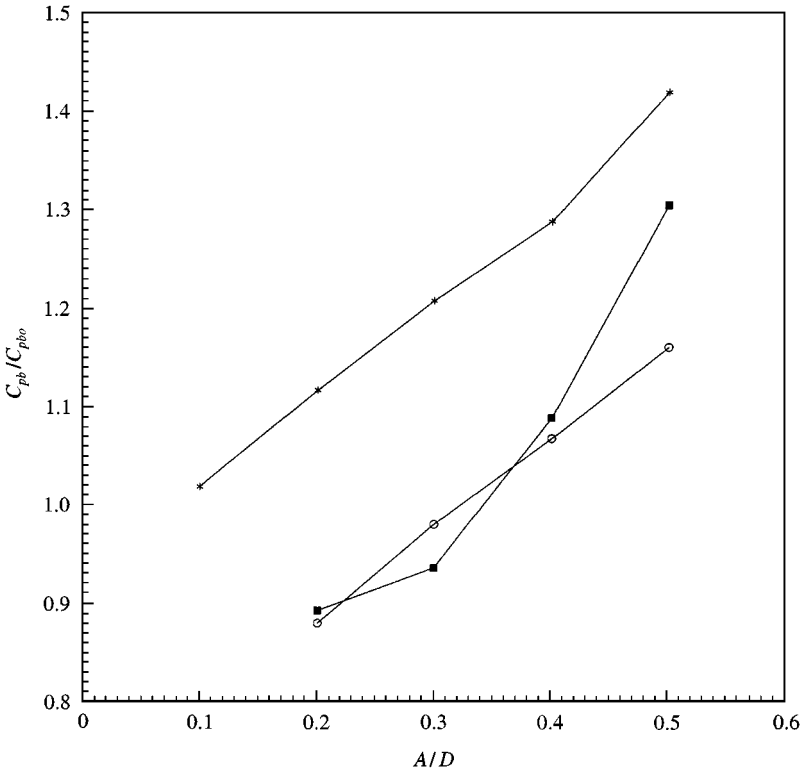

Figure 25. Variation of base pressure with the oscillation amplitude: –○–, $f_c/f_s = 0{\cdot}80$; –∗–, $f_c/f_s = 1{\cdot}00$; –■–, $f_c/f_s = 1{\cdot}10$.

aperiodic at subsequent cycles, except from the case in which the oscillation amplitude is equal to 50% of a cylinder diameter. It was shown that this aperiodicity is initiated by an instability in the near-wake, due to the coexistence of two saddle points in the streamline pattern, in the instant when the cylinder displacement becomes maximum. In spite of this cycle-to-cycle intermittence, periodicity is established at a certain number of cycles, as concluded from long time records. This reinforces strongly the argument posed in Part 1 of the study, that the modulation in the force and velocity traces is the result of an aperiodicity in the wake, and not necessarily a manifestation of unlocked conditions.

The circulation shed into the wake per oscillation cycle increases as the oscillation frequency is reduced, whereas it increases with increasing oscillation amplitude, when the oscillation frequency is maintained constant. The maximum strength of the vortices also increases as the oscillation amplitude is increased at constant frequency, in a way that the ratio of maximum circulation surviving in the wake to that shed per cycle remains almost constant. As the oscillation amplitude increases at a constant frequency, the position of maximum vortex strength moves downstream until A/D becomes 0·30 and then it is almost stabilized, while the point of maximum u'_{rms} on the wake centreline migrates continually towards the cylinder. The point of maximum u'_{rms} on the wake centreline at high oscillation amplitudes gives a measure of the first appearance of the vortices, and does not seem to constitute a criterion for the formation length as in the case when the cylinder remains fixed.

The absolute value of base pressure increases as the oscillation frequency is increased at constant amplitude, undergoes a sudden drop at $f_r = 1$ and then rises again. Also, the

absolute base pressure becomes higher when the oscillation amplitude is increased at a constant frequency.

The present results seem to be qualitatively similar to those expected at higher Reynolds numbers in the subcritical regime. Comparison of the lock-in boundary derived herein with experimental studies at higher Reynolds numbers reveals a reasonable agreement, especially for $f_r < 1$. Moreover, the results regarding the behaviour of the mean drag and base pressure with oscillation amplitude and frequency changes follow the same trend, although the magnification of the mean drag is greater at higher Reynolds numbers. A difference seems to occur in the phase angle, which, at higher Reynolds numbers, displays a sharp decrease as the oscillation frequency is increased near resonance. In the present study, this abrupt jump was observed only for $A/D = 0{\cdot}10$, whereas, the phase angle decrease was substantially milder at higher oscillation amplitudes.

References

Akbari, M. H. & Price, S. J. 1997 Simulation of the incompressible viscous cross-flow around an oscillating circular cylinder via the random vortex method. In *Proceedings of the Fourth International Symposium on Fluid–Structure Interactions, Aeroelasticity, Flow-Induced Vibration and Noise* (eds M. P. Paidoussis *et al.*), Vol. 1, pp. 21–32. New York: ASME.

Anagnostopoulos, P. 1997a Numerical study of the effects of the transverse cylinder oscillation on the laminar wake. In *Proceedings of the Fourth International Symposium on Fluid–Structure Interactions, Aeroelasticity, Flow-Induced Vibration and Noise* (eds M. P. Paidoussis *et al.*), Vol. 1, pp. 11–19. New York: ASME.

Anagnostopoulos, P. 1997b Computer-aided flow visualization and vorticity balance in the laminar wake of a circular cylinder. *Journal of Fluids and Structures*, **11,** 33–72.

Anagnostopoulos, P. 2000 Numerical study of the flow past a cylinder excited transversely to the incident stream. Part 1. Hydrodynamic forces and wake geometry. *Journal of Fluids and Structures* **14,** 819–851, doi:10.1006/jfls.2000.0302.

Bishop, R. E. D. & Hassan, A. Y. 1964 The lift and drag forces on a circular cylinder oscillating in a flowing fluid. *Proceedings of the Royal Society of London*, series A **277,** 51–75.

Copeland, G. S. & Cheng, B. H. 1995 Hysteretic vortex shedding form an oscillating cylinder. In *Proceedings of the Sixth International Conference on Flow-Induced Vibration* (ed. P. W. Bearman), pp. 221–230, London, U.K. Rotterdam: A. A. Balkema.

Green, R. B. & Gerrard, J. H. 1991 An optical interferometric study of the wake of a bluff body. *Journal of Fluid Mechanics* **226,** 219–242.

Griffin, O. M. 1971 The unsteady wake of an oscillating cylinder at low Reynolds number. *Journal of Applied Mechanics* **38,** 729–738.

Griffin, O. M. & Ramberg, S. E. 1974 The vortex-street wakes of vibrating cylinders. *Journal of Fluid Mechanics* **66,** 553–576.

Gu, W., Chyu, C. & Rockwell, D. 1994 Timing the vortex formation from an oscillating cylinder. *Physics of Fluids* **6,** 3677–3682.

Honji, H. & Taneda, S. 1968 Vortex wakes of oscillating circular cylinders. *Reports of Research Institute for Applied Mechanics, Kyushu* **16,** 211–222.

Koopmann, G. H. 1967 The vortex wakes of vibrating cylinders at low Reynolds numbers. *Journal of Fluid Mechanics* **27,** 501–512.

Lu, X.-Y. & Dalton, C. 1996 Calculation of the timing of vortex formation from an oscillating cylinder. *Journal of Fluids and Structures* **10,** 527–541.

Meneghini, J. R. & Bearman, P. W. 1995 Numerical simulation of high amplitude oscillatory flow about a circular cylinder. *Journal of Fluids and Structures* **9,** 435–455.

Ongoren, A. & Rockwell, D. 1988 Flow structure from an oscillating cylinder. Part 1: mechanisms of phase shift and recovery in near wake. *Journal of Fluid Mechanics* **191,** 197–223.

Perry, A. E., Chong, M. S. & Lim, T. T. 1982 The vortex-shedding process behind two-dimensional bluff bodies. *Journal of Fluid Mechanics* **116,** 77–90.

Stansby, P. K. 1976 Base pressure of oscillating circular cylinders. *ASCE Journal of the Engineering Mechanics Division* **102,** 591–600.

Williamson, C. H. K. & Roshko, A. 1988 Vortex formation in the wake of an oscillating cylinder. *Journal of Fluids and Structures* **2,** 355–381.